NASA Technical Memorandum 101698

Flow Visualization Study of a 1/48-Scale AFTI/F111 Model to Investigate Horizontal Tail Flow Disturbances

Lisa J. Bjarke
Ames Research Center, Dryden Flight Research Facility, Edwards, California

1990

NASA

CONTENTS

ABSTRACT

During flight testing of the AFTI/F111 aircraft, horizontal tail buffet was observed. Flutter analysis ruled out any aeroelastic instability, so a water-tunnel flow visualization study was conducted to investigate possible flow disturbances on the horizontal tail which might cause buffet. For this study, a 1/48-scale model was used. Four different wing cambers and one horizontal tail setting were tested between 0°- and 20°-angle of attack. These wing cambers corresponded to the following leading–trailing-edge deflections: 0/2, 10/10, 10/2, and 0/10. Flow visualization results in the form of still photographs are presented for each of the four wing cambers between 8°- and 12°-angle of attack. In general, the horizontal tail experiences flow disturbances which become more pronounced with angle of attack or wing trailing-edge deflection.

INTRODUCTION

The NASA Ames Research Center, Dryden Flight Research Facility (Ames-Dryden) and the United States Air Force have been flight testing the AFTI/F111 mission adaptive wing (MAW) research aircraft. This aircraft is an F-111 testbed that has been modified to accept an MAW. The MAW replaces conventional high lift and lateral control devices with a three-segment, smooth-camber trailing edge and a single-segment, smooth-camber leading edge. By eliminating gaps and slots associated with conventional devices, the smooth-camber devices will provide a significant drag reduction. More information about the concept can be found in Bonnema and Smith (1988).

During the initial flight testing, a low-frequency, high-amplitude vibration was observed on the horizontal tail. After flutter analysis, it was determined that this vibration was not caused by aeroelastic or aeroservoelastic instability. It was suspected that some form of separated flow, perhaps a vortex originating from the wing or fuselage, was causing a flow disturbance over the horizontal tail.

To investigate this problem, a water-tunnel test was conducted at the Ames-Dryden Flow Visualization Facility. Flow visualization tests using water as the medium have historically provided insight to researchers about certain aerodynamic flow phenomena. Typically they are convenient and economical to use. However, flow rates are low which result in low Reynolds numbers (on the order of 20,000/ft to 100,000/ft) compared to flight. When modeling attached flow, it is important to match the Reynolds number. However in this study, the angles of attack (α) of interest were greater than or equal to 8° where the flow regime can be dominated by separation or vortex flow. According to Erickson (1981), this regime is less sensitive to Reynolds number and therefore the use of the water tunnel was deemed appropriate.

A 1/48-scale model was used for this study. Four sets of wings were tested: 1) 0°-leading-edge deflection, 2°-trailing-edge deflection, 2) 10°-leading and trailing-edge deflections, 3) 10°-leading-edge deflection, 2°-trailing-edge deflection, and 4) 0°-leading-edge deflection, 10°-leading-edge deflection. The cruise and maneuver configurations, 0/2 and 10/10 respectively, were the configurations where tail buffet had been experienced in flight. The other two configurations were tested to determine how much (if any) other wing leading- or trailing-edge deflection combinations had on the flow. Still photograph results are presented in this paper for each camber configuration at 8°-, 10°-, and 12°-angle of attack and one horizontal tail position.

NOMENCLATURE

AFB	air force base
AFTI	advanced fighter technology integration
Ames-Dryden	Ames Research Center, Dryden Flight Research Facility
M	Mach number

MAW	mission adaptive wing
R_n	unit Reynolds number, ft^{-1}
$\bar{q}$	dynamic pressure, lb/ft^2
V_o	water tunnel velocity, in/s
i_h	horizontal tail position, positive trailing edge down, deg
α	model angle of attack, deg
β	model angle of sideslip, deg
$\delta_{LE/TE}$	leading–trailing-edge camber deflection, positive down, deg
Λ_{LE}	leading-edge sweepback angle, deg
$\delta_{LE/TE} = 0/2$	cruise camber configuration
$\delta_{LE/TE} = 10/10$	maneuver camber configuration

APPARATUS AND PROCEDURE

Water-Tunnel Facility

The Ames-Dryden Flow Visualization Facility was used for the AFTI/F111 test. It is a single-return facility with a 16-in. by 24-in. test section (fig. 1). The walls of the test section are made of clear plexiglass 2-in. thick. The velocity in the test section can be varied from .5 to 18 in/s corresponding to unit Reynolds numbers of 4000 to 138,600/ft. The model is supported on a 3/8-in. sting and angle of attack can be changed using an external crank. Sideslip (β) can be varied by mounting the model on the sting using an angled adaptor. If the model is equipped with flow-through inlets, mass flow can be simulated. The primary flow visualization technique is dye injection from ports on the model. A more detailed description of the facility can be found in Hall and Del Frate (1986).

Model Description

The 1/48-scale model used for this test was constructed by the Air Force at Wright Patterson AFB. Figure 2 is a photograph of the model. The fuselage and tail were constructed using automotive bondo and the wings were fabricated from fiberglass. The model also incorporated flow-through inlets to simulate mass flow through the engines.

Since horizontal tail buffet had been observed in flight for the cruise configuration camber, $\delta_{LE/TE} = 0/2$ and the maneuver configuration camber, $\delta_{LE/TE} = 10/10$ (Friend, 1989), these two sets of MAWs were initially fabricated and tested. After testing these wings, it was decided that two more configurations should be tested to separate out the effects of other leading- and trailing-edge deflections. The two additional sets of wings were $\delta_{LE/TE} = 10/2$ and $\delta_{LE/TE} = 0/10$ camber.

On each side of the model, there were three internal dye ports on the wing glove, three internal dye ports on the $\delta_{LE/TE}$ 0/2 and $\delta_{LE/TE}$ 10/10 wings, and four internal dye ports on the $\delta_{LE/TE}$ 10/2 and $\delta_{LE/TE}$ 0/10 wings (fig. 3). The dye ports on the wing glove and the $\delta_{LE/TE}$ 0/2 and $\delta_{LE/TE}$ 10/10 wings were not located in the same place on each side (fig. 3(a)). This asymmetric placement was done to visualize different portions of the model on each side. However this arrangement turned out to be rather confusing, so the $\delta_{LE/TE}$ 10/2 and $\delta_{LE/TE}$ 0/10 wings were built with symmetric dye port locations (fig. 3(c)).

There were three externally routed dye lines: one up the lower fuselage center line of the aircraft stopping just under the cockpit area, the second along the underside of the right horizontal tail stopping at the leading edge of the root, and the third went through the right inlet stopping at the inlet lip (fig. 3(b)).

2

Test Conditions

The test conditions for the results presented are shown in Table 1. The wing sweep was 26° for this study, which is the wing sweep used in flight for the subsonic speed range. The $-10°$-horizontal tail position is shown since it is most representative of flight trim conditions for the angles of attack being tested. Only one inlet flow rate was tested, which corresponded to a flight inlet capture area ratio for $M = 0.7$ and $\bar{q} = 300$ lb/ft^2.

RESULTS AND DISCUSSION

The analysis presented was made from both still photographs and video recordings. Only the still photographs are included in this report, although useful information about the flow dynamics was obtained from the video recordings to assist in the analysis.

Selected results will be presented and discussed for each of the four configurations. The conditions selected for presentation were between 8°- and 12°-angle of attack with a horizontal tail position of $-10°$. This position is most representative of flight trim position for these angles of attack.

Cruise Camber Configuration $\delta_{LE/TE} = 0/2$

Figures 4 through 6 present flow visualization results obtained for the $\delta_{LE/TE} = 0/2$ camber configuration at $\alpha = 8°,10°$, and 12° respectively. This configuration is representative of cruise flight conditions. Three primary flow features should be noted in the flow field: wing flow separation, a glove vortex, and an inlet lip–fuselage juncture vortex.

At $\alpha = 8°$, the plan view (fig. 4(a)) shows that wing flow separation occurs just behind the leading-edge devices. The glove vortex burst point is near the wing root at approximately mid-chord. (It should be noted that the path of this vortex and its effect on the flow over the wing agreed with wind-tunnel tuft flow visualization results from a Boeing study summarized by Nelson (1982)). The side view (fig. 4(b)) shows that the wing separation and glove vortex flow goes above the horizontal tail while the lower surface of the horizontal tail experiences a different flow field. This type of flow field on the horizontal tail could be the cause of the slight horizontal tail buffet experienced in flight at similar test conditions as discussed by Friend (1989). Also visible in the side view is a weak vortex that begins at the engine inlet lip–fuselage juncture, travels aft along the fuselage and causes a flow disturbance both above and below the horizontal tail root.

Figure 5 presents the flow visualization results at $\alpha = 10°$ for this configuration. With the increase in angle of attack, flow separation on the wing moved slightly forward (fig. 5(a)). In addition, there is now both a primary and secondary glove vortex, both of which burst slightly further forward on the wing than at $\alpha = 8°$ (fig. 4(a)). In the side view (fig. 5(b)), the separated and vortex flow field from the wing can again be seen traveling above the horizontal tail. However, at this angle of attack, more of the inlet lip vortex goes beneath the horizontal tail than at $\alpha = 8°$ (fig. 4(b)).

At $\alpha = 12°$, (fig. 6(a)), more of the wing is separated, especially inboard. This is because the burst point of the secondary glove vortex has moved forward to the wing–glove juncture. The primary vortex is stronger but its burst point is at approximately the same place as it was at $\alpha = 10°$ (fig. 5(a)). Most of the inlet lip vortex curves down away from the wing as it travels aft and goes under the horizontal tail (fig. 6(b)).

Maneuver Camber Configuration $\delta_{LE/TE} = 10/10$

Figures 7 through 9 show the results for the maneuver camber configuration $\delta_{LE/TE} = 10/10$, at $\alpha = 8°$, 10°, and 12° respectively. The three primary flow features mentioned previously are visible for this configuration. Although

wing flow separation is further aft for this configuration (figs. 7(a), 8(a), and 9(a)), it still moves forward with increasing angle of attack as was discussed previously. The glove vortex follows similar behavior for this configuration as for the $\delta_{LE/TE}$ = 0/2 configuration.

The side views (figs. 7(b), 8(b), and 9(b)) show that the separated and glove vortex flow from the wing still travel above the horizontal tail but turns downward near the trailing-edge device and interact more directly with the horizontal tail upper surface. The inlet lip vortex appears more circulatory (stronger) in nature and interacts directly with the horizontal tail at the root leading edge. This difference is most dramatic at α = 10° and 12° (figs. 8(b) and 9(b)) where the inlet lip vortex engulfs the horizontal tail rather than traveling on one side or the other as was the case when $\delta_{LE/TE}$ = 0/2 (figs. 5(b) and 6(b)). With the changes in the direction and placement of both the flow from the wing and the inlet lip, the horizontal tail is in a more disturbed flow field at $\delta_{LE/TE}$ = 10/10 than at $\delta_{LE/TE}$ = 0/2. These results are consistent with the findings of Friend (1989) which show increased horizontal tail buffet experienced in flight for similar test conditions.

Camber Configuration $\delta_{LE/TE}$ = 10/2

Figures 10 through 12 present the flow visualization results for the $\delta_{LE/TE}$ = 10/2 camber configuration. This configuration had different dye port locations on the wing than the first two configurations discussed. In addition, alternating colors were used on the wing.

Generally, in comparing this configuration to the previous two configurations discussed, the wing separation and glove vortex burst location (figs. 10(a), 11(a), and 12(a)) behaved similarly to that of $\delta_{LE/TE}$ = 10/10 (figs. 7(a), 8(a), and 9(a)). However, the side views (figs. 10(b), 11(b), and 12(b)) indicate that the direction of the separated and glove vortex flow are more similar to that of the $\delta_{LE/TE}$ = 0/2 configuration (figs. 4(b), 5(b), and 6(b)). From these results it appears that the horizontal tail is subject to similar flow fields at both $\delta_{LE/TE}$ = 0/2 and 10/2.

Camber Configuration $\delta_{LE/TE}$ = 0/10

Figures 13 through 15 show the results for the $\delta_{LE/TE}$ = 0/10 camber configuration. The behavior of the location of flow separation and glove vortex burst point (figs. 13(a), 14(a), and 15(a)) follow similar trends like those discussed for all the previous cases.

By looking at the side views for this configuration (figs. 13(b), 14(b), and 15(b)), it is noted that the path that the separated and glove vortex flow takes is most similar to that of the $\delta_{LE/TE}$ 10/10 camber configuration (figs. 7(b), 8(b), and 9(b)); that is, a downward turn near the trailing edge causing a more direct interaction with the horizontal tail. The inlet lip vortex also has direct interaction with the horizontal tail, especially at α = 12° (fig. 15(b)).

CONCLUDING REMARKS

A water-tunnel test was conducted on a 1/48-scale model of the AFTI/F111 aircraft. The purpose of this test was to investigate the causes of horizontal tail buffet experienced in flight-test. Four wing cambers were tested: $\delta_{LE/TE}$ = 0/2, 10/10, 10/2, and 0/10. Results were presented for α = 8°, 10°, and 12° with a wing sweep of 26° and a horizontal tail position of −10°.

In general, the results of this study indicate that the horizontal tail experiences flow disturbances. These flow disturbances become more pronounced with increased angle of attack or trailing-edge deflection and are consistent with the buffet trends experienced in flight.

The flow disturbances are attributed to the following:

1. The glove vortex burst over the wing and mixed with the wing separated flow which traveled above the horizontal tail,

2. The inlet lip–fuselage juncture vortex traveled aft along the horizontal tail,

3. Increased trailing-edge device deflection causes the separated and glove vortex flow to turn downward and interact more directly with the horizontal tail.

These horizontal tail disturbances occurred at test conditions which are consistent with the flight-test buffet results.

REFERENCES

Bonnema, K.L. and S.B. Smith, AFTI/F-111 Mission Adaptive Wing Flight Research Program, AIAA 88-2118, May 1988.

Erickson, G.E., Vortex Flow Correlation, AFWAL-TR-80-3143, Jan. 1981.

Friend, E.L., Buffett Characteristics of the AFTI/F-111 with the Maneuver Adaptive Wing, AFTI/F-111 Symposium Paper, NASA CP-3055, 1989.

Hall, Capt. R.M. and J.H. Del Frate, Interaction Between Forebody and Wing Vortices — A Water Tunnel Study, AFWAL-TM-85-252, Jan. 1986.

Nelson, D.W., AFTI/F111 Mission Adaptive Wing Wind Tunnel Analysis Report, Test Entry III, NARC 449-1-12 and NARC 449-1-11T, D365- 10074-1, The Boeing Company, Mar, 1982.

Table 1. Test conditions.

	$\delta_{LE/TE}$, deg			
	0/2	10/10	10/2	0/10
α, deg	8	8	8	8
	10	10	10	10
	12	12	12	12

$V_o = 3$ in/s
$R_n \approx 23,000$/ft
$\Lambda_{LE} = 26°$
$\beta = 0°$
$i_h = -10°$
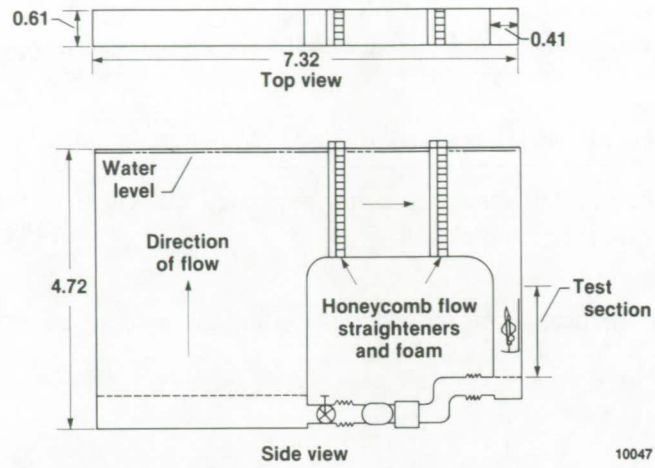
(a) Water-tunnel schematic (dimensions in meters).
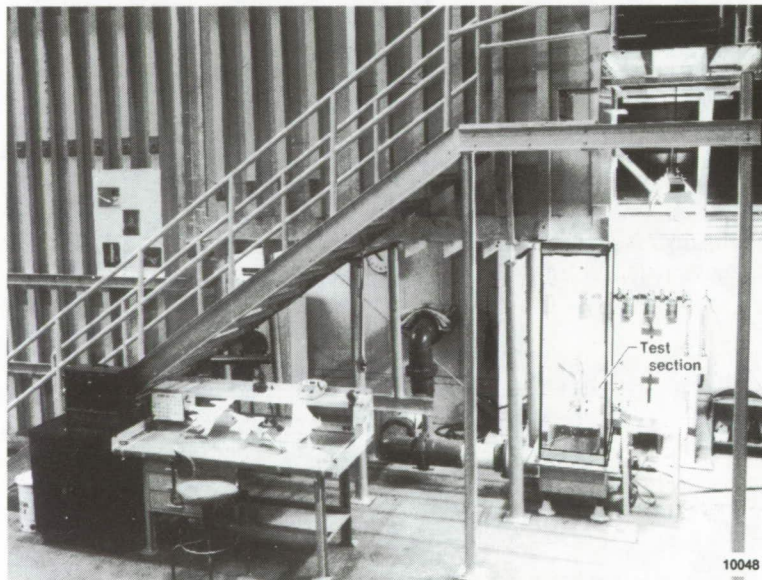
(b) Conventional test setup of water tunnel.

Figure 1. Ames-Dryden flow visualization system.
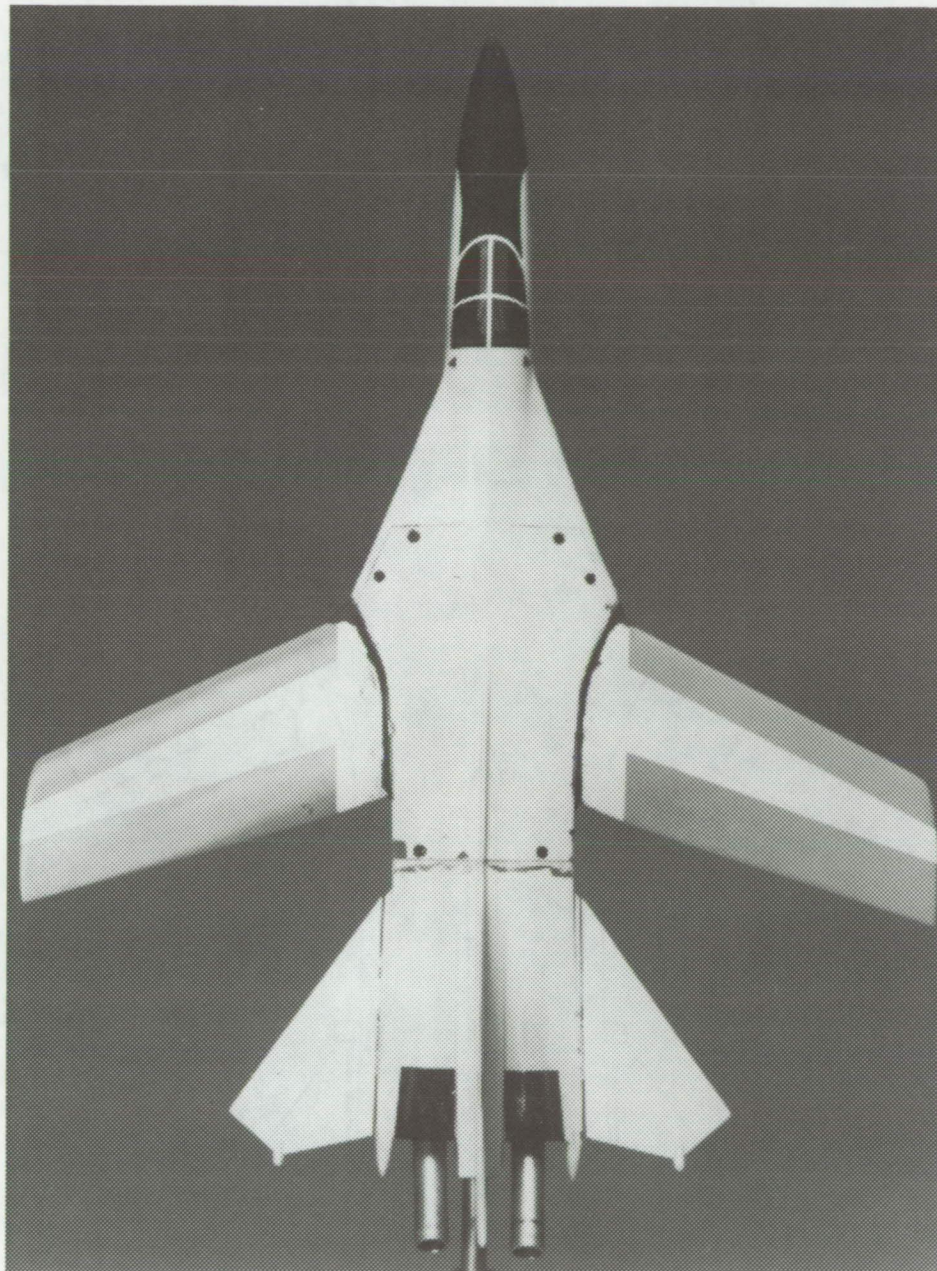
EC89-0031-001

Figure 2. Water-tunnel model with the $\delta_{LE/TE} = 0/2$ wings installed.

Wing glove

Leading-edge
device

Trailing-edge
device
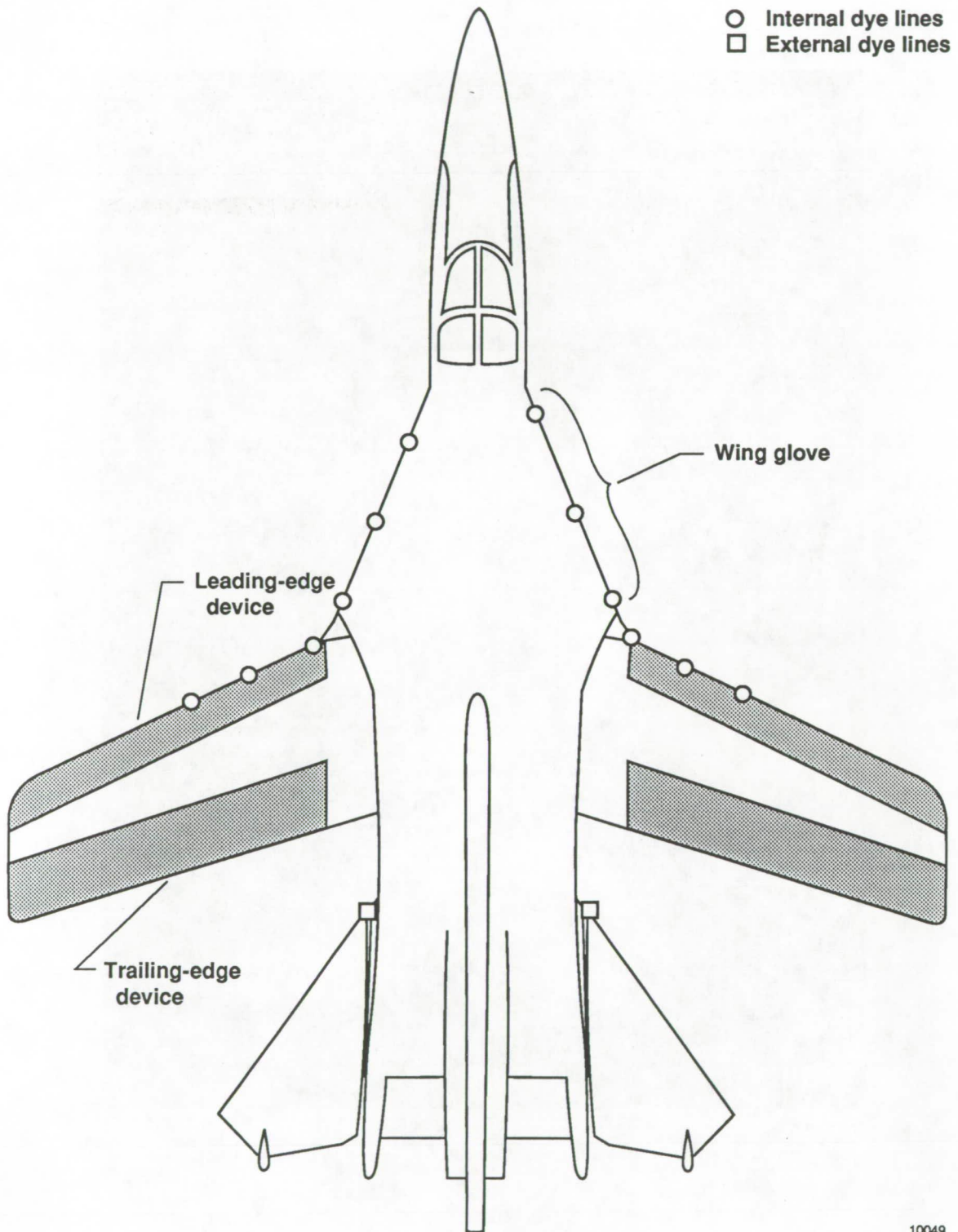
10049

(a) Plan view $\delta_{LE/TE} = 0/2$ and 10/10.

Figure 3. Dye port locations.

O Internal dye lines
□ External dye lines
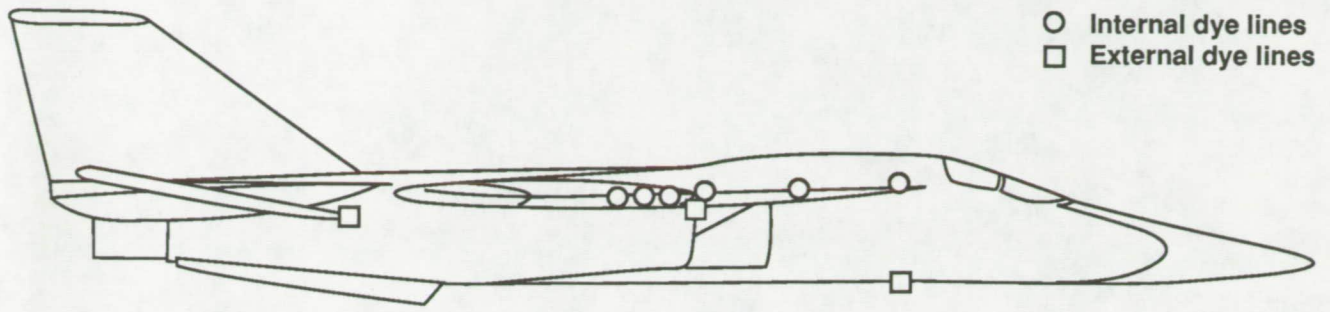
10050
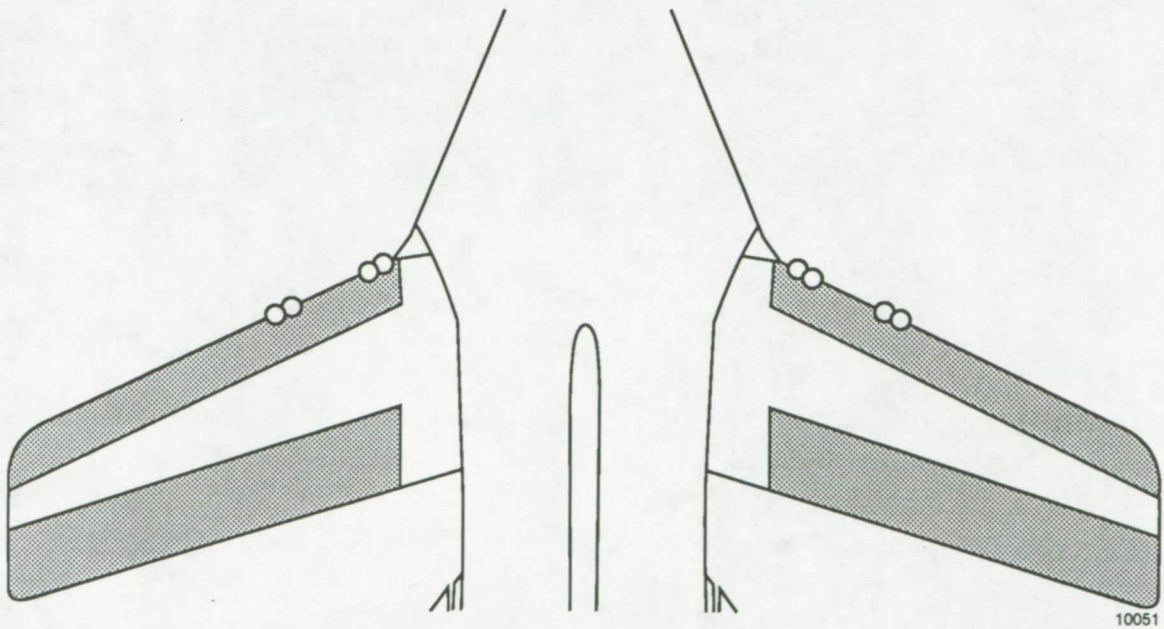
(b) Side view.

10051

(c) Plan view $\delta_{LE/TE}$ = 10/2 and 0/10.

Figure 3. Concluded.
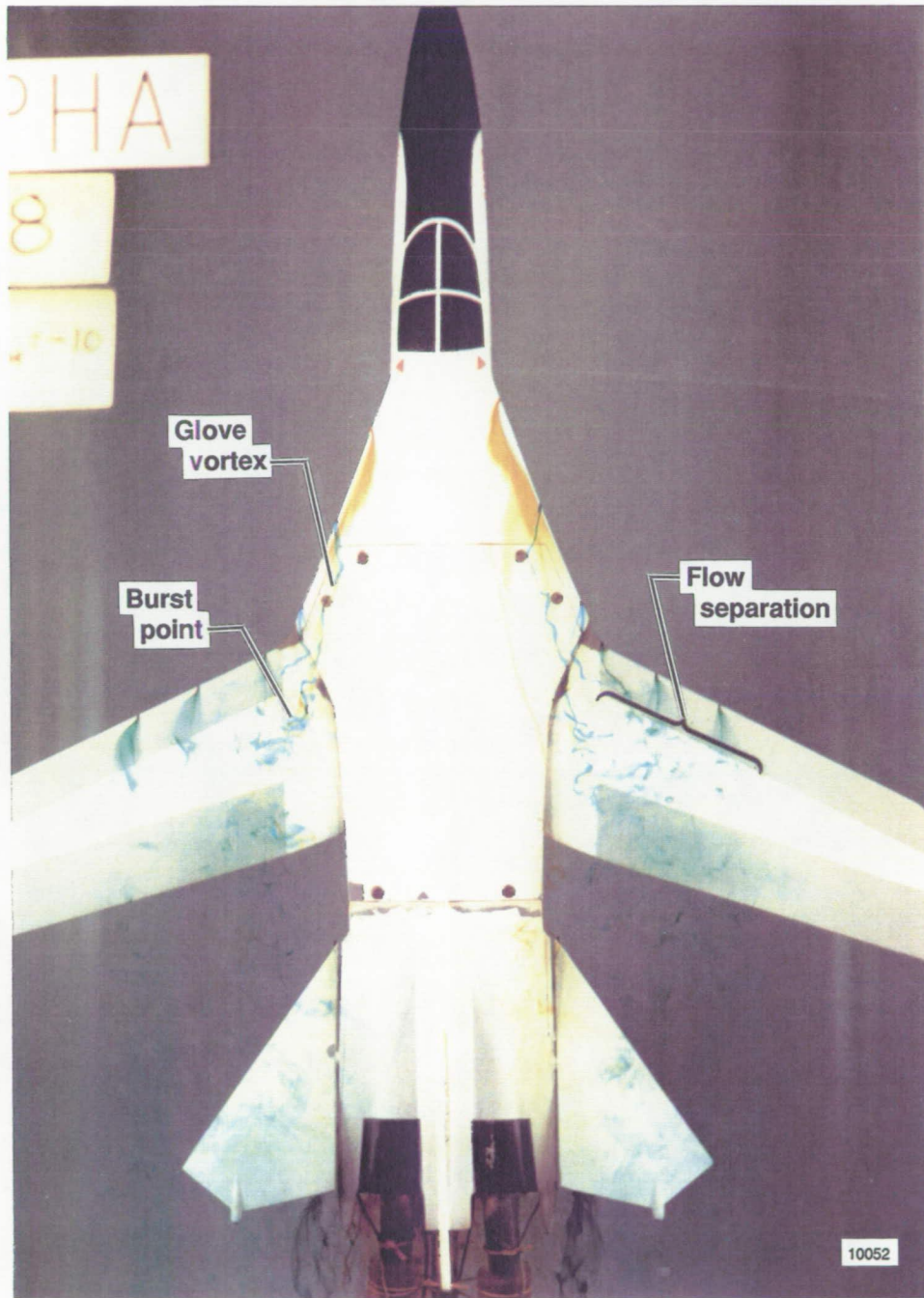
(a) Plan view.

Figure 4. Characteristic flow patterns at $\alpha = 8°$, $\delta_{LE/TE} = 0/2$, and $i_h = -10°$.
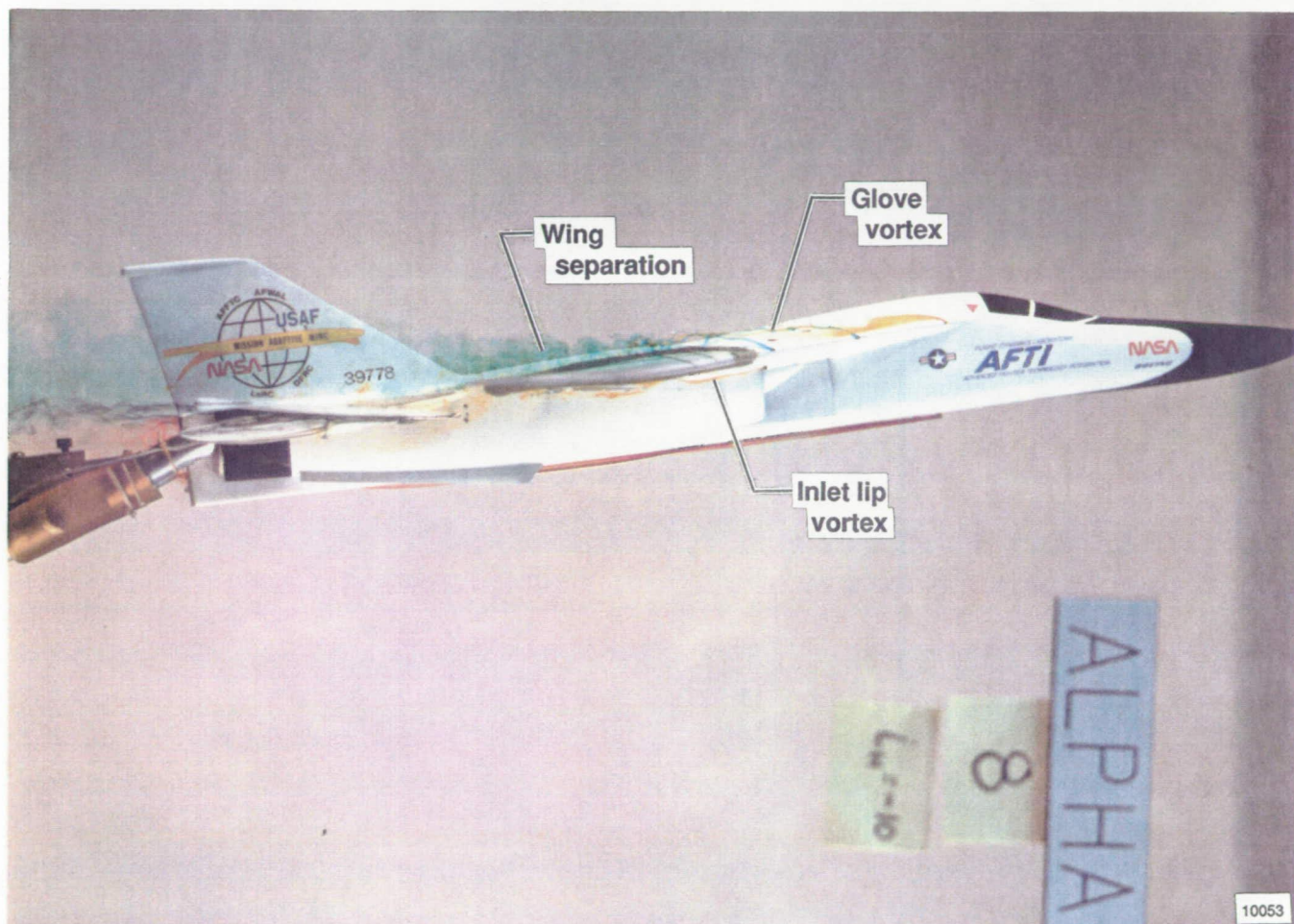
(b) Side view.

Figure 4. Concluded.
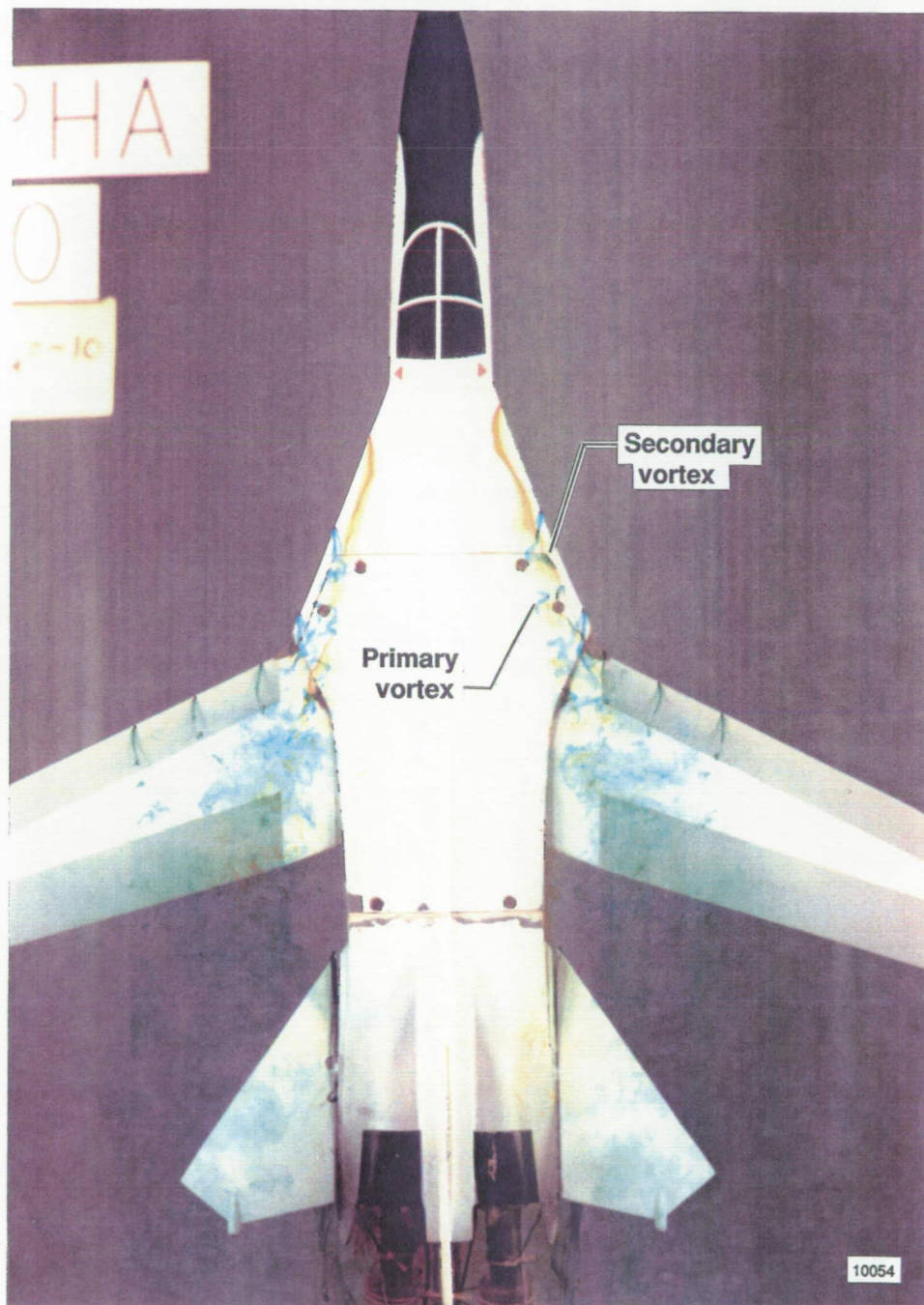
(a) Plan view.

Figure 5. Characteristic flow patterns at $\alpha = 10°$, $\delta_{LE/TE} = 0/2$, and $i_h = -10°$.
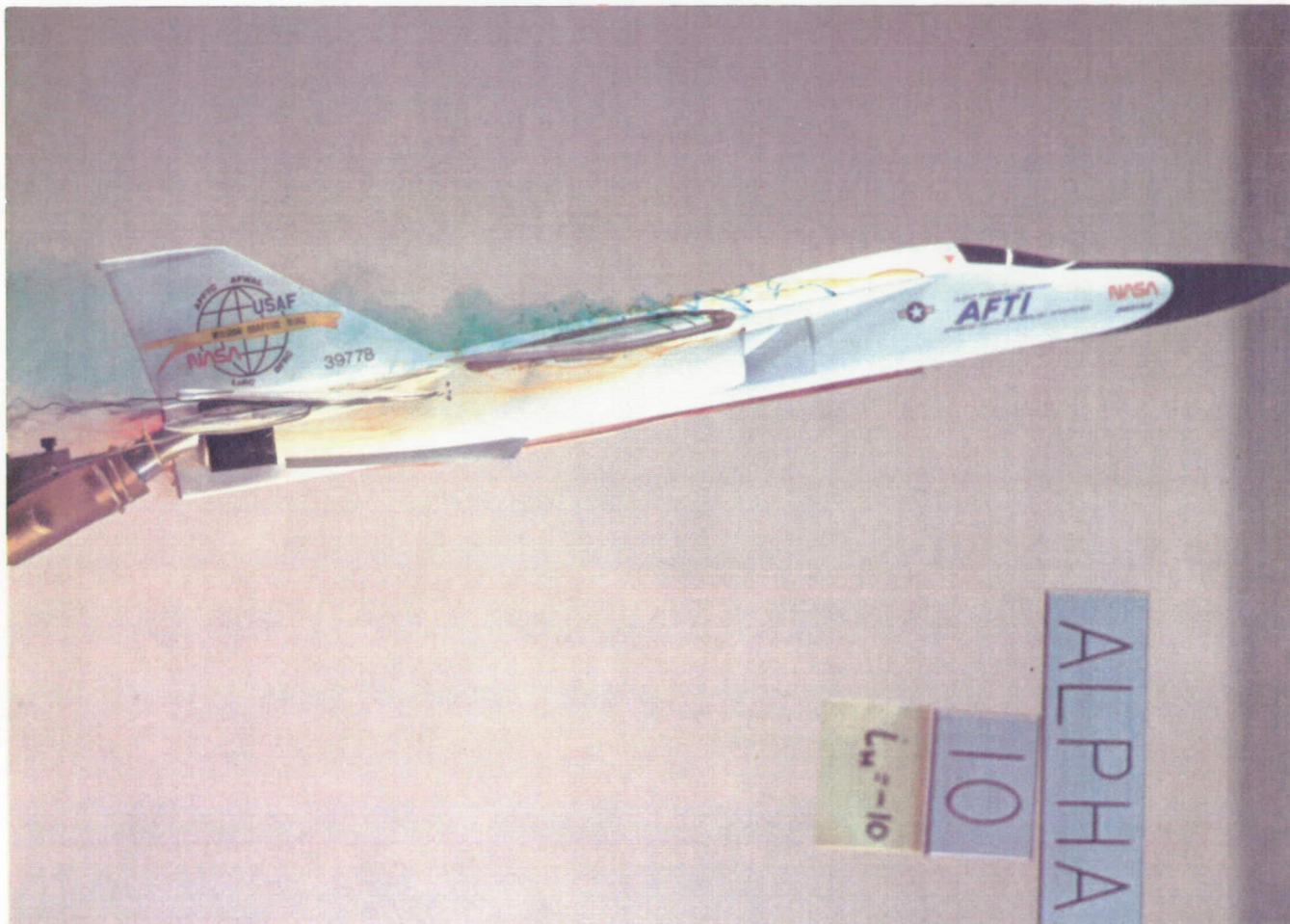
EC90 143-1

(b) Side view.

Figure 5. Concluded.
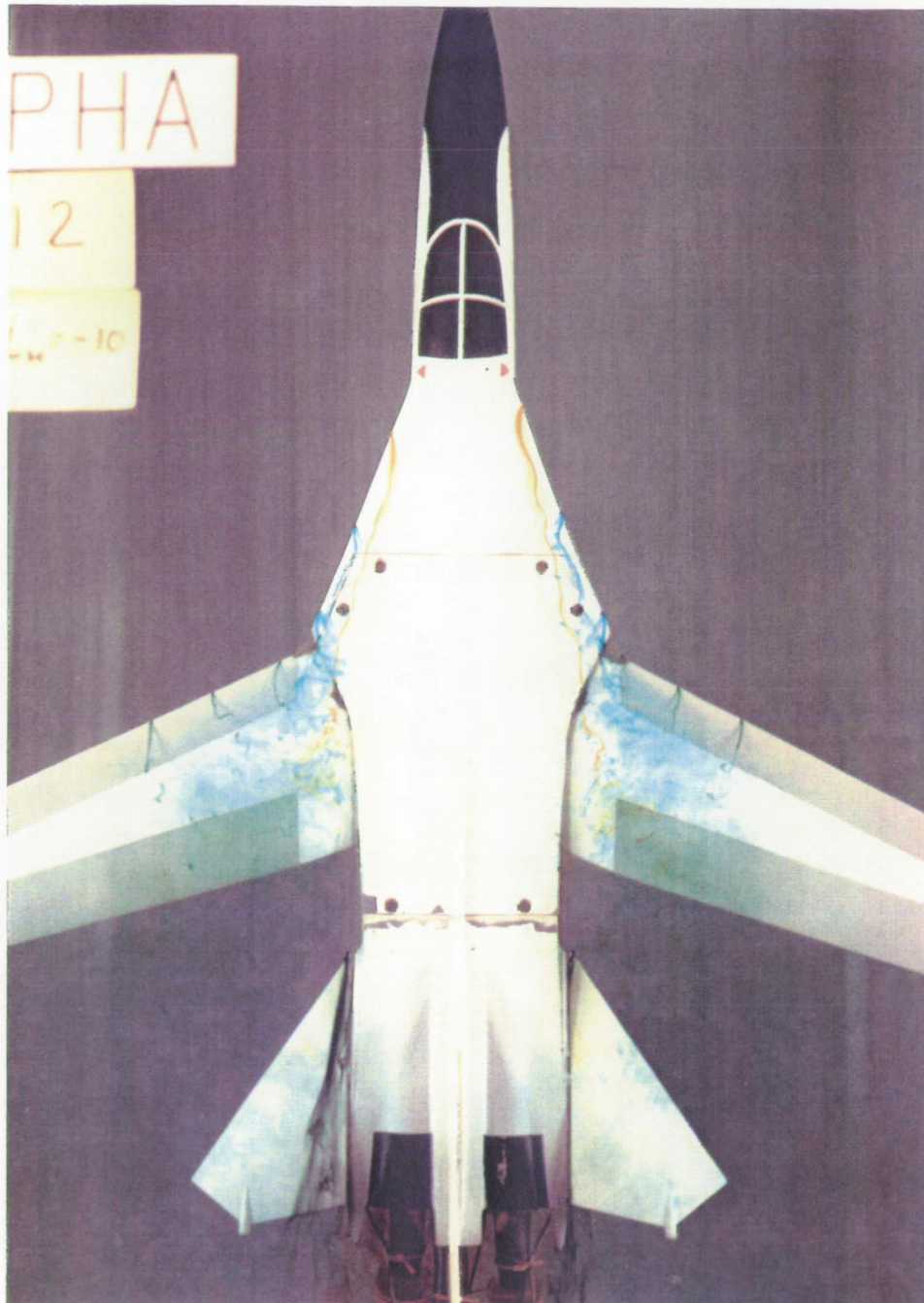
EC90 143-3

(a) Plan view.

Figure 6. Characteristic flow patterns at $\alpha = 12°$, $\delta_{LE/TE} = 0/2$, and $i_h = -10°$.
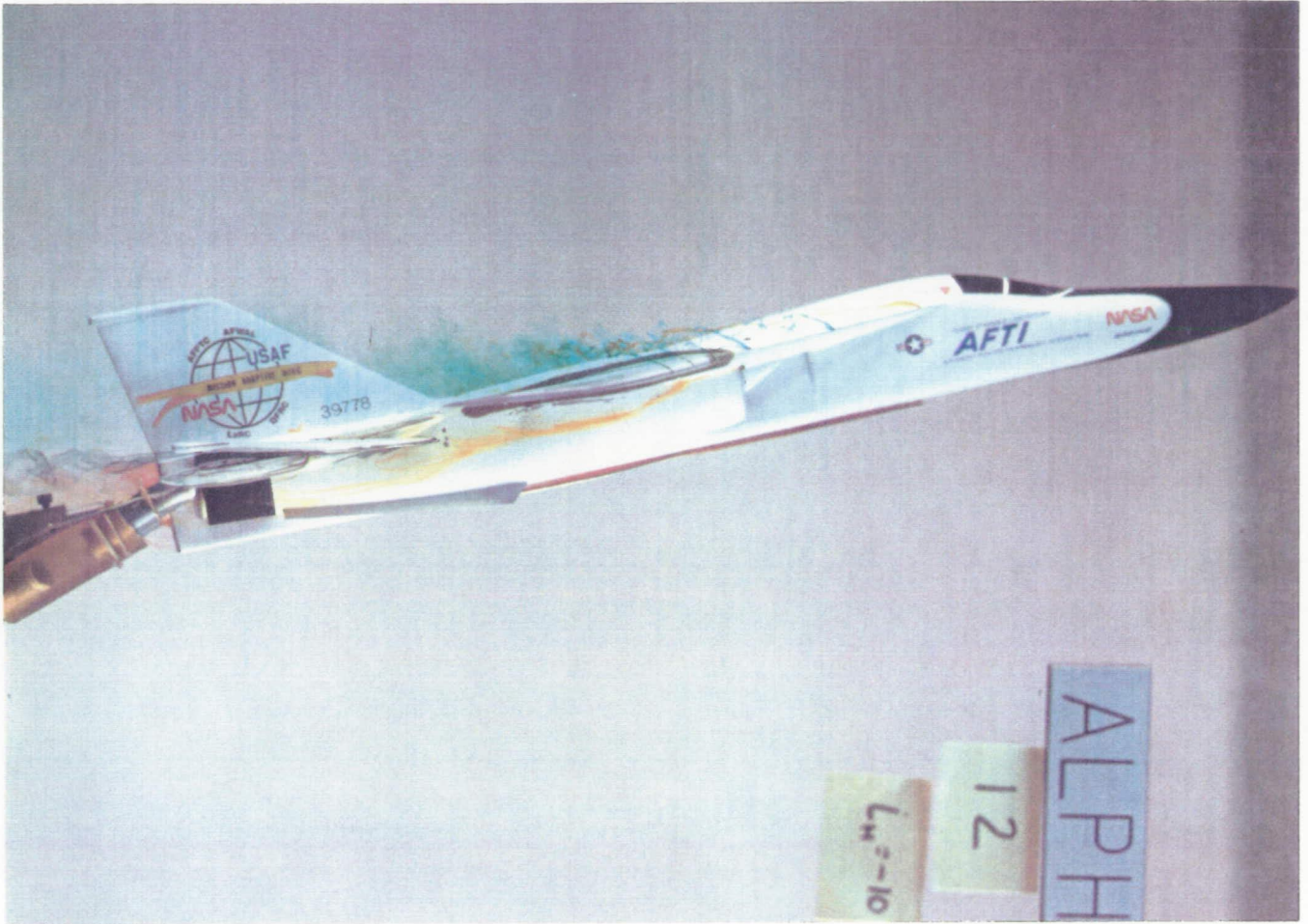
EC90 143-2

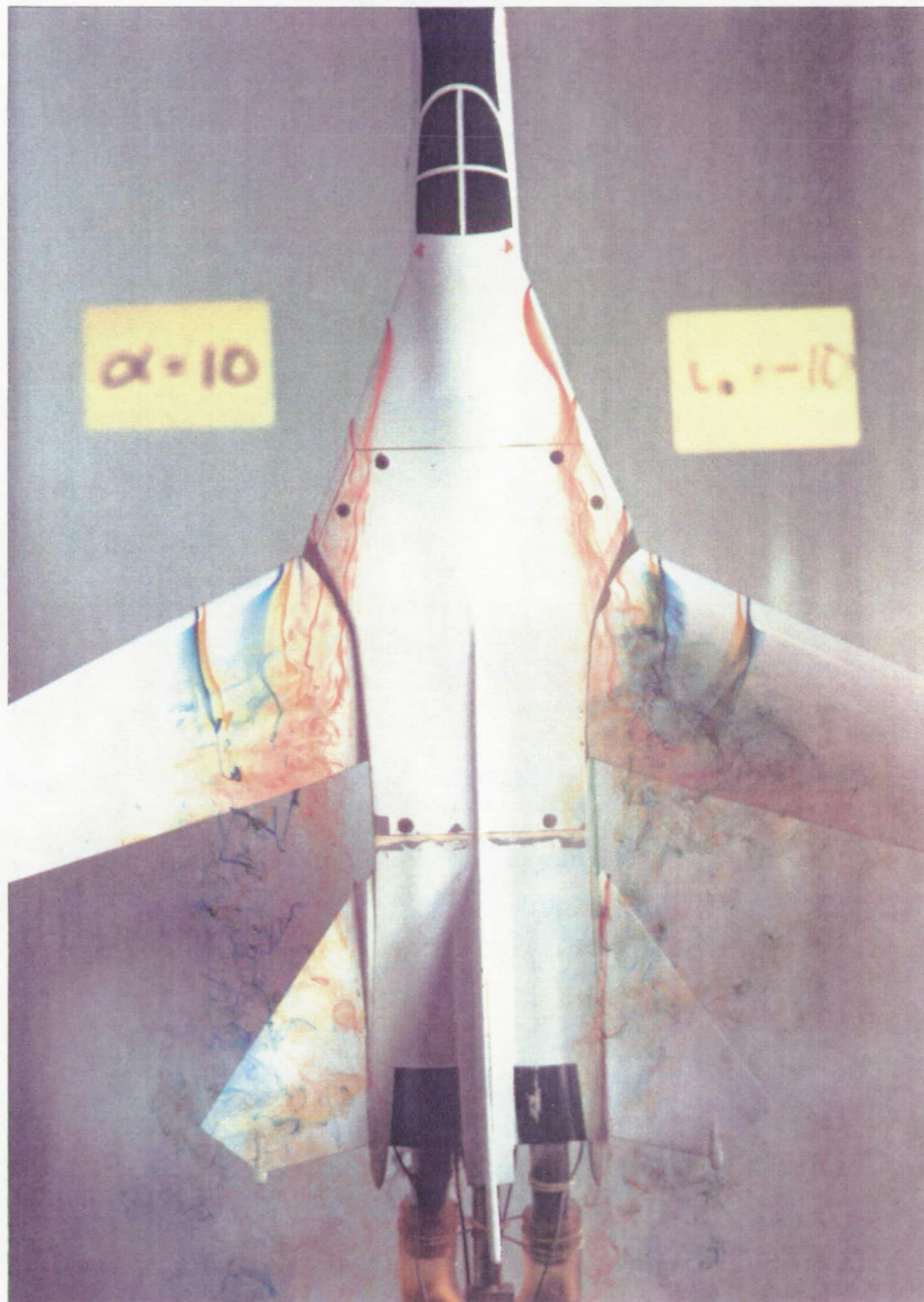(b) Side view.

Figure 6. Concluded.
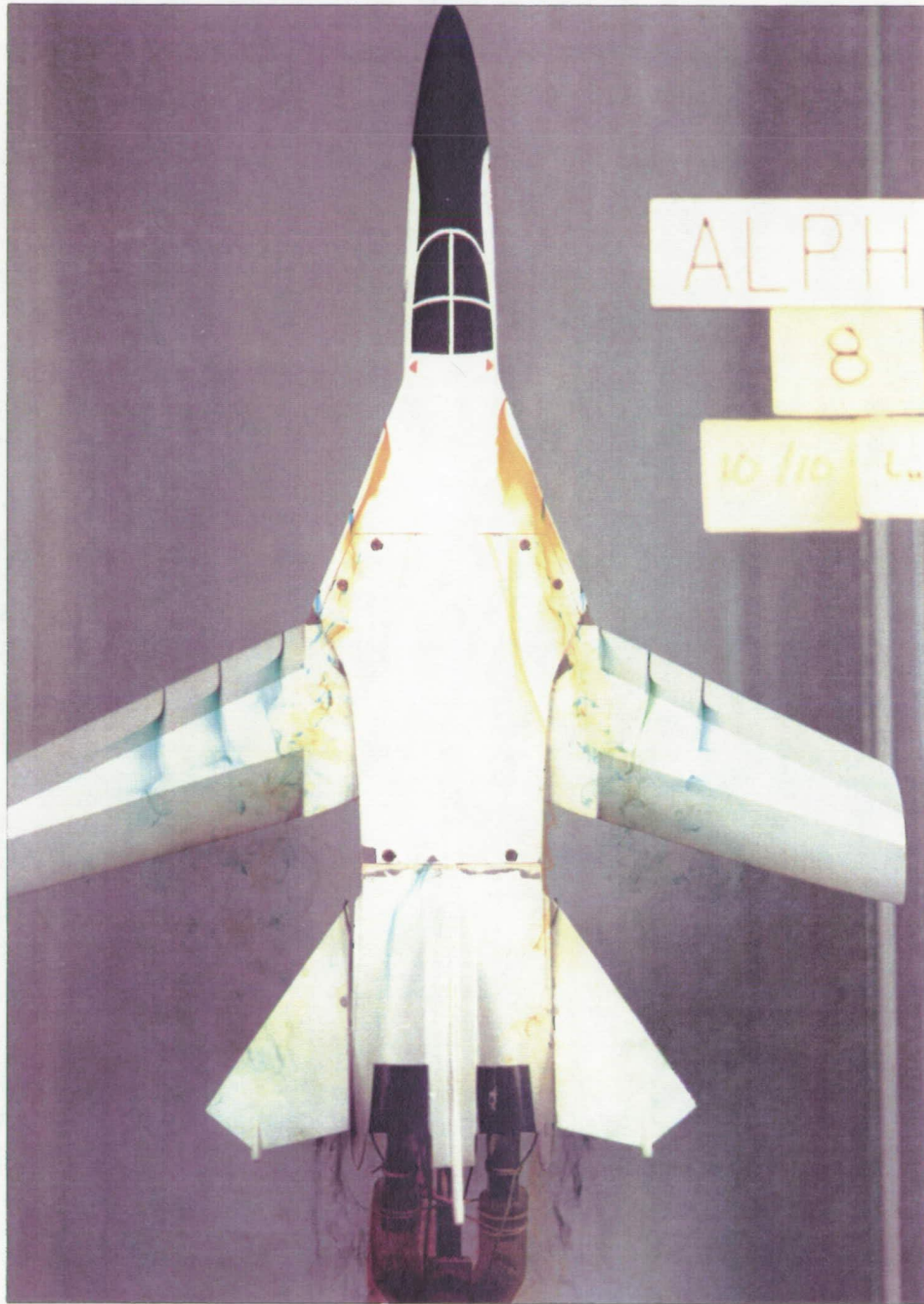
EC90 143-4

(a) Plan view.

Figure 7. Characteristic flow patterns at $\alpha = 8°$, $\delta_{LE/TE} = 10/10$, and $i_h = -10°$.
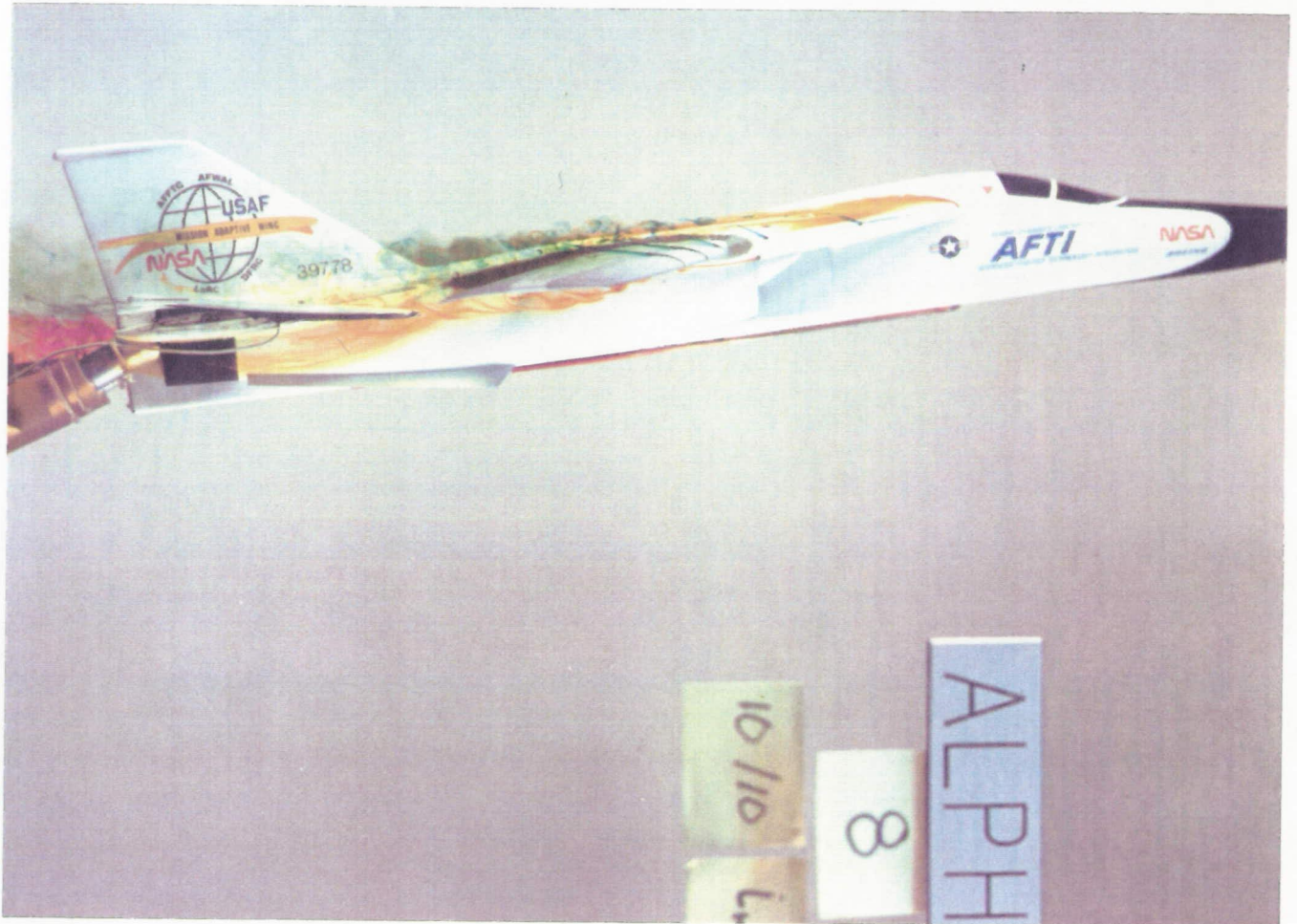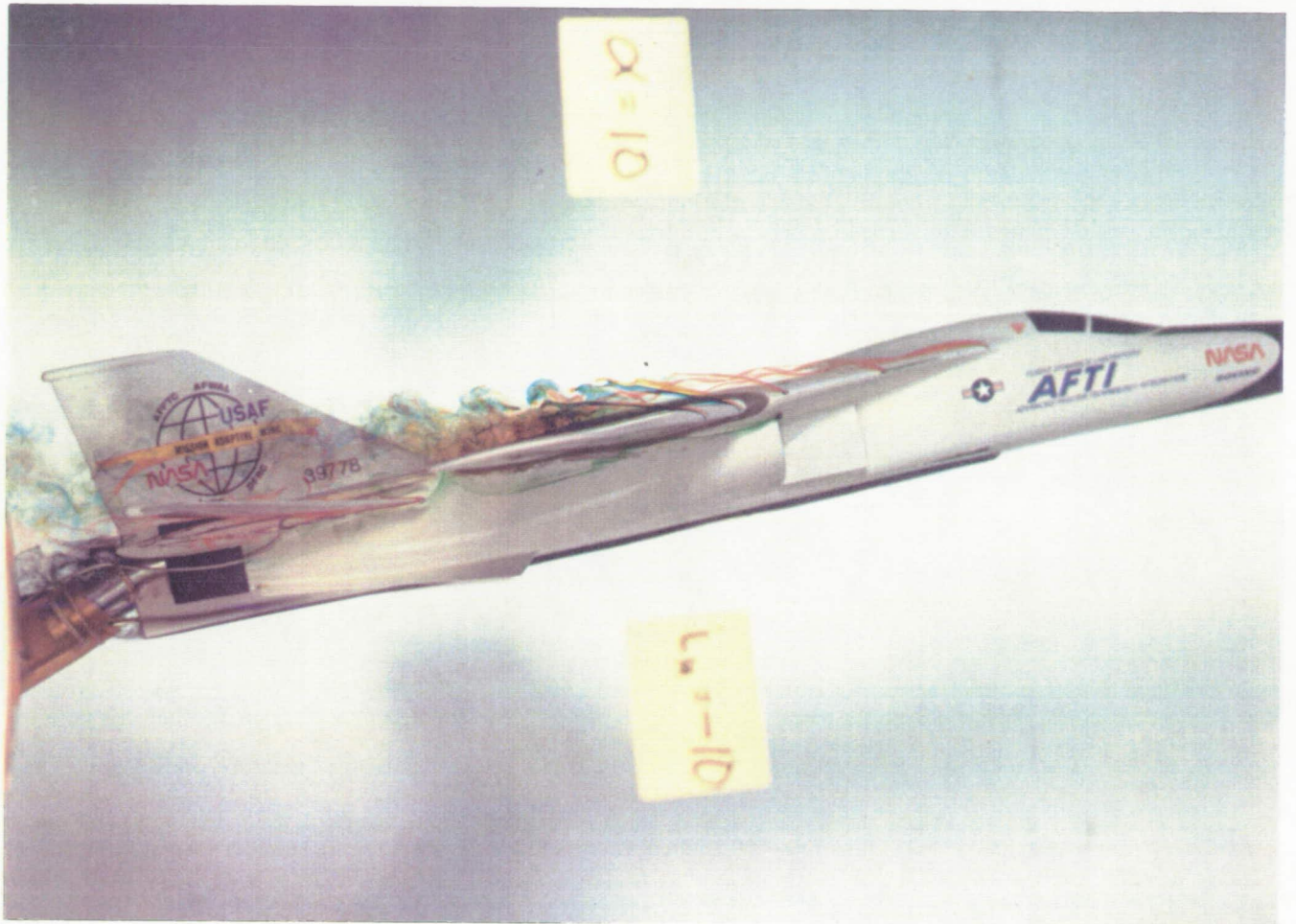
EC90 143-6

(b) Side view.

Figure 7. Concluded.
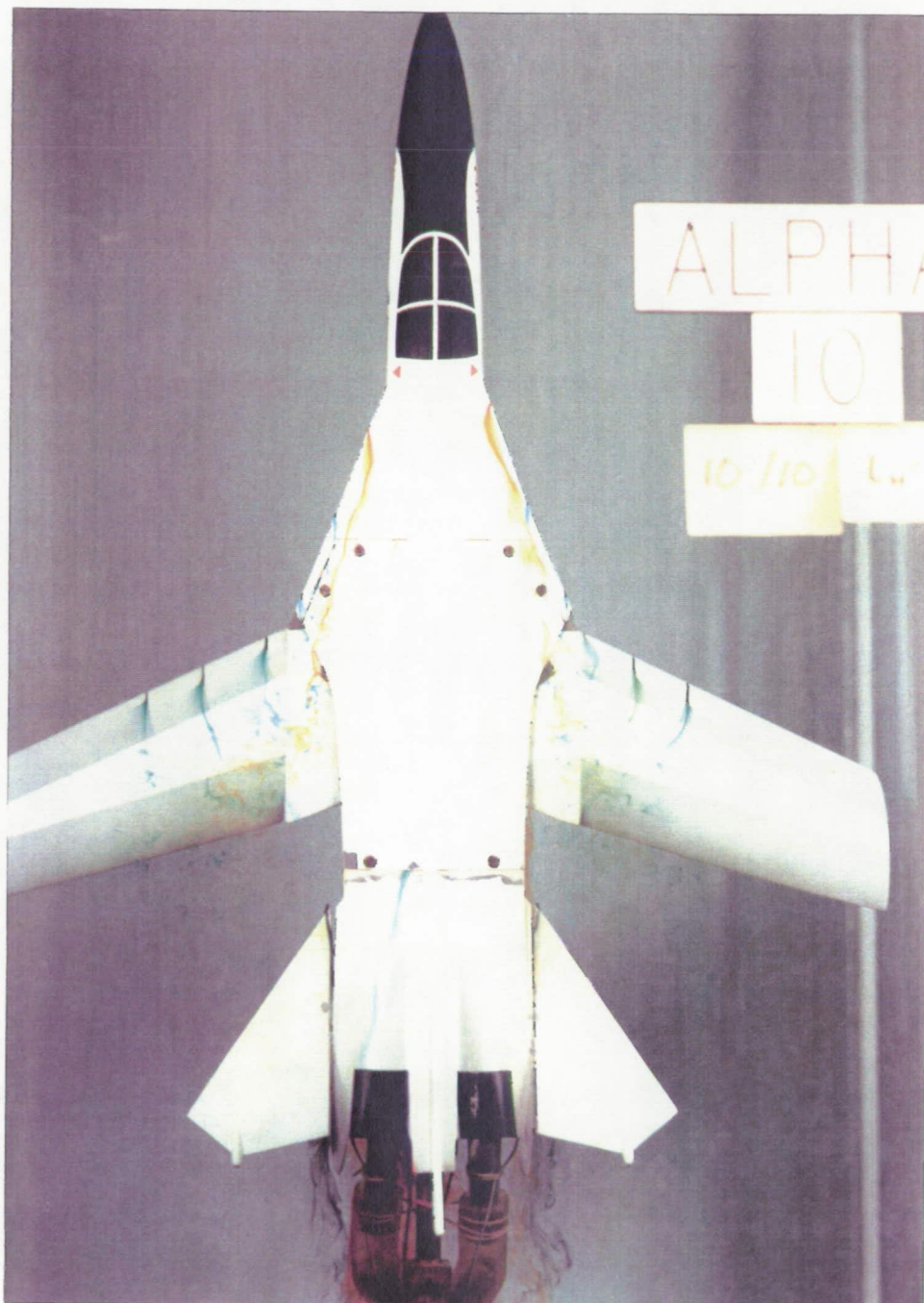
EC90 143-8

(a) Plan view.

Figure 8. Characteristic flow patterns at $\alpha = 10°$, $\delta_{LE/TE} = 10/10$, and $i_h = -10°$.
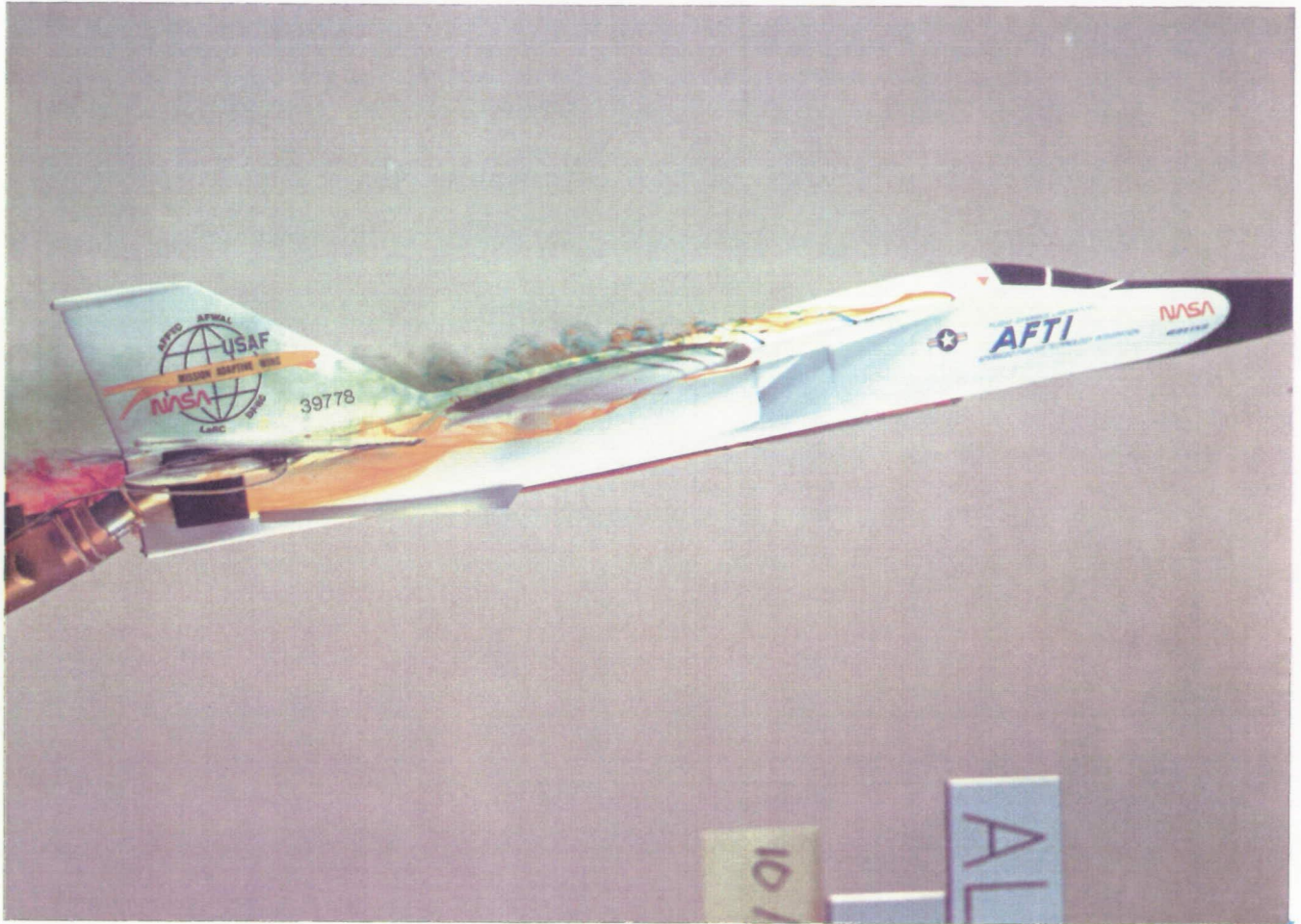
EC90 143-5

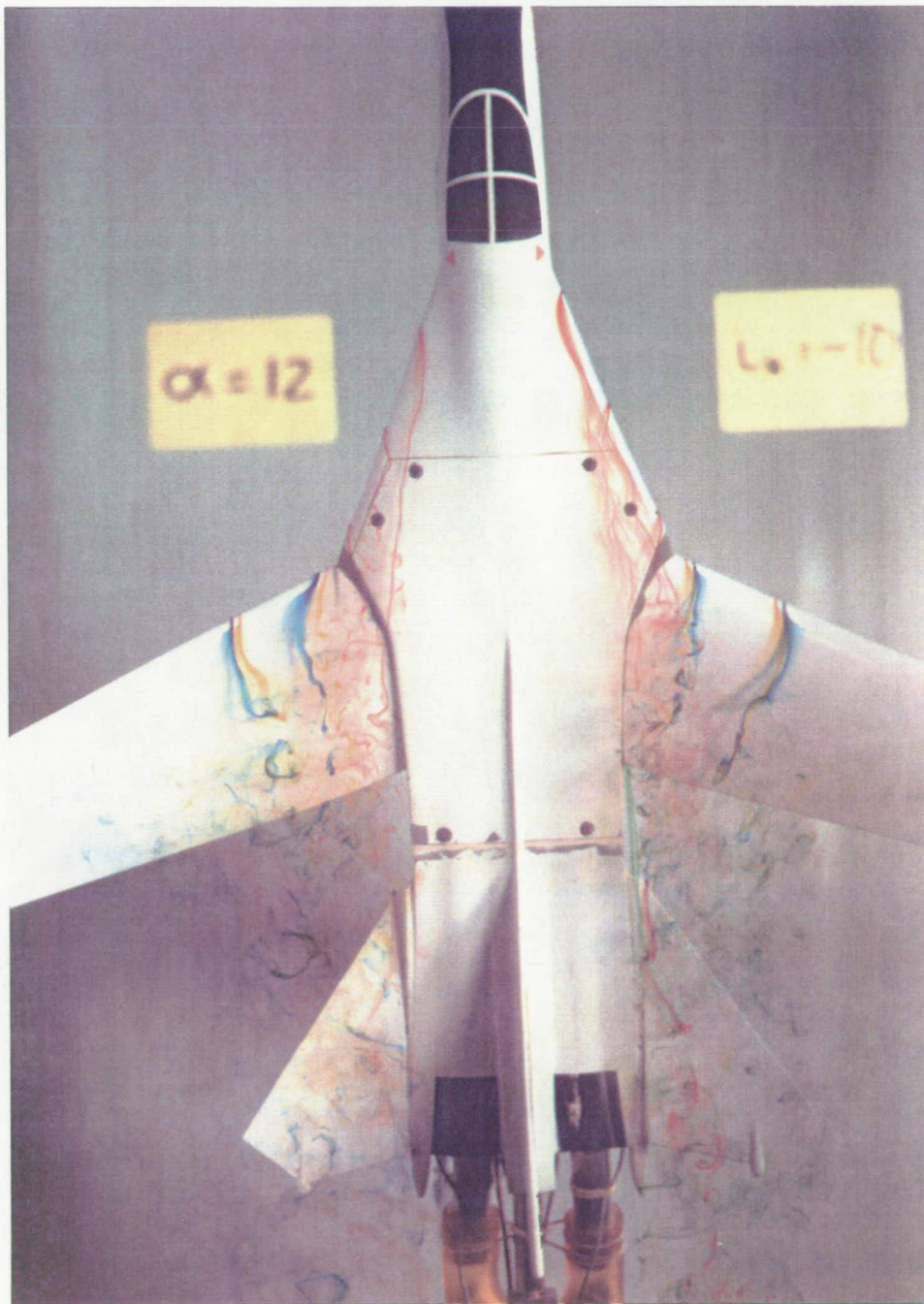(b) Side view.
Figure 8. Concluded.
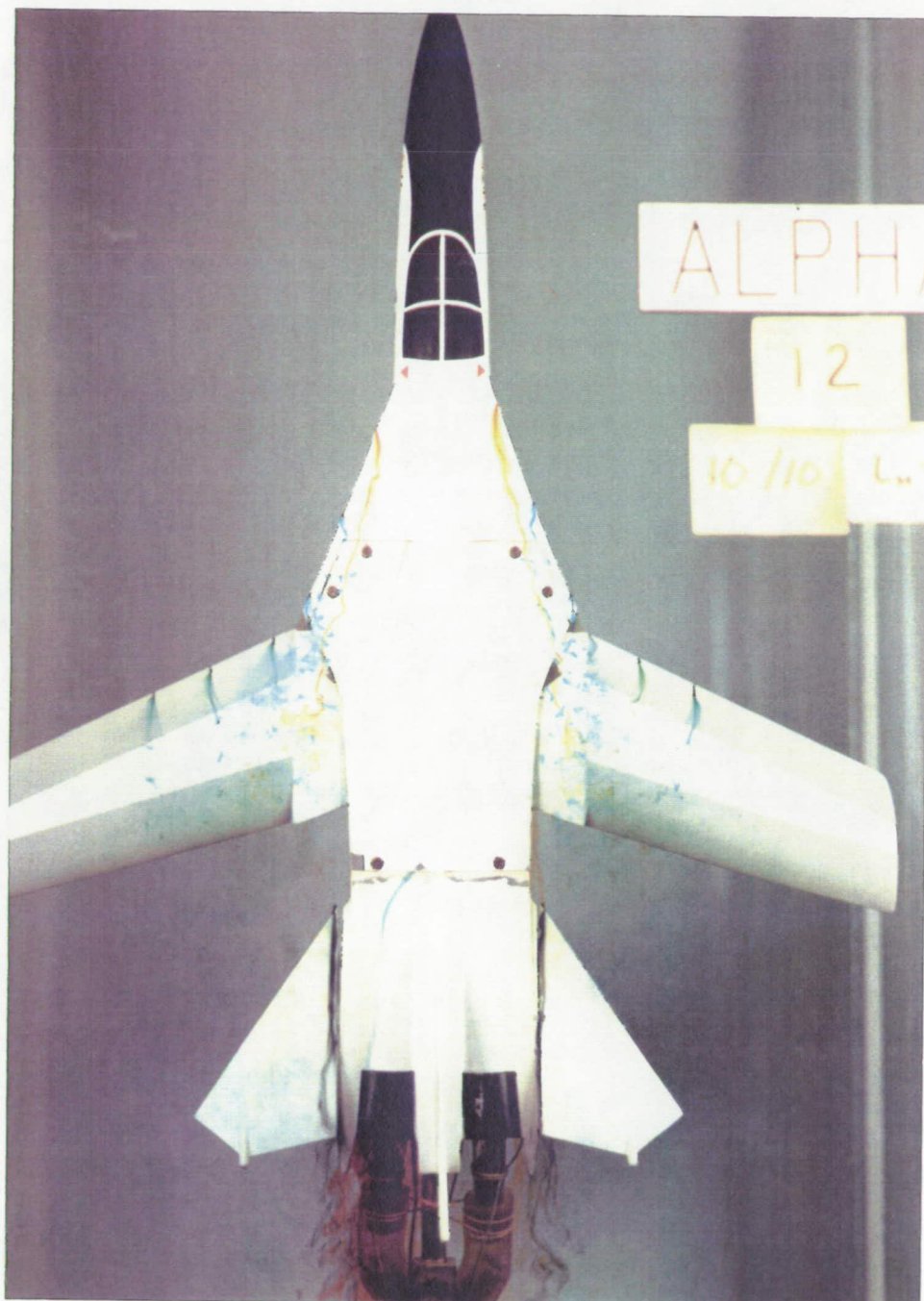
EC90 143-7

(a) Plan view.

Figure 9. Characteristic flow patterns at $\alpha = 12°$, $\delta_{LE/TE} = 10/10$, and $i_h = -10°$.
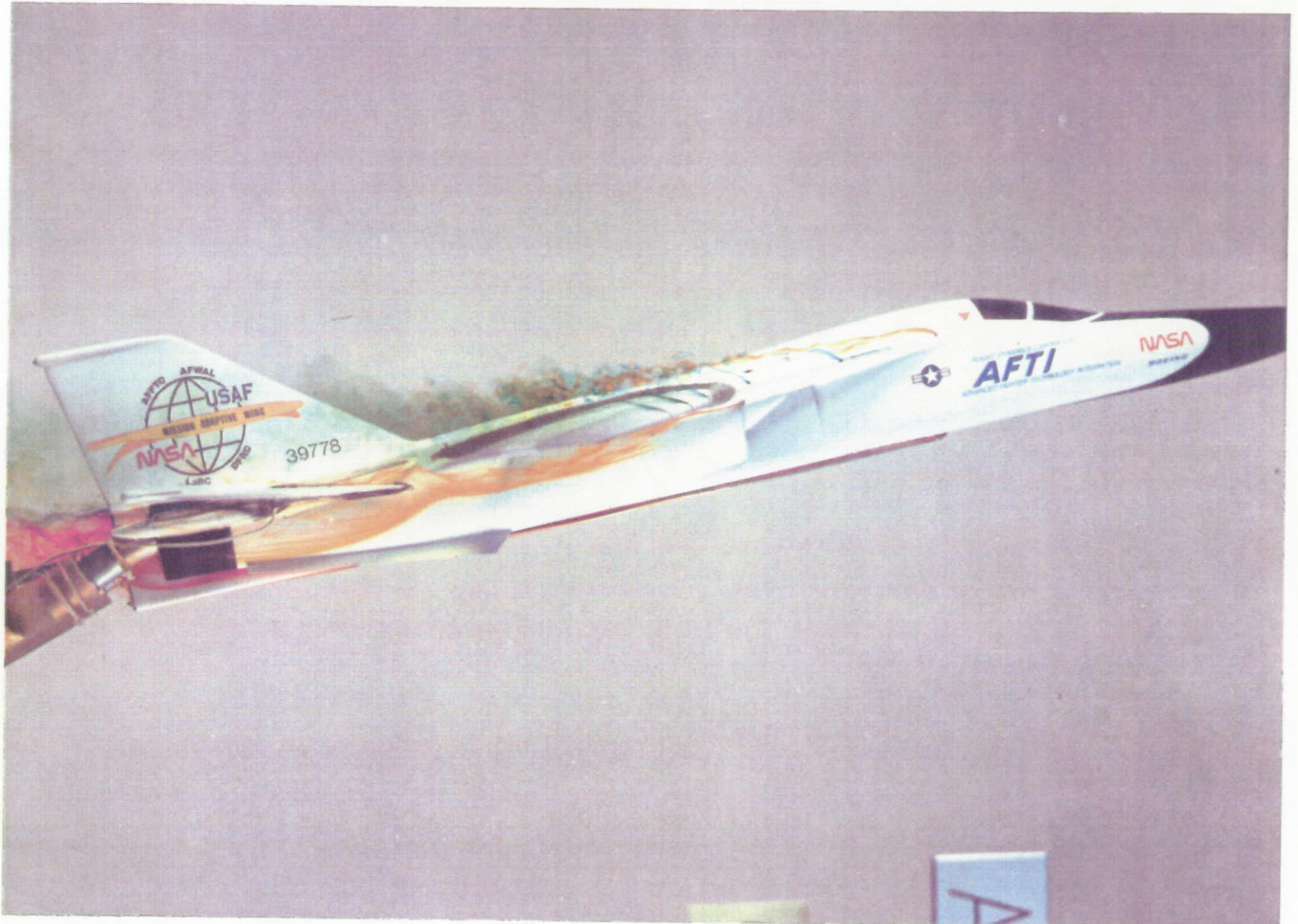
EC90 143-9

(b) Side view.
Figure 9. Concluded.
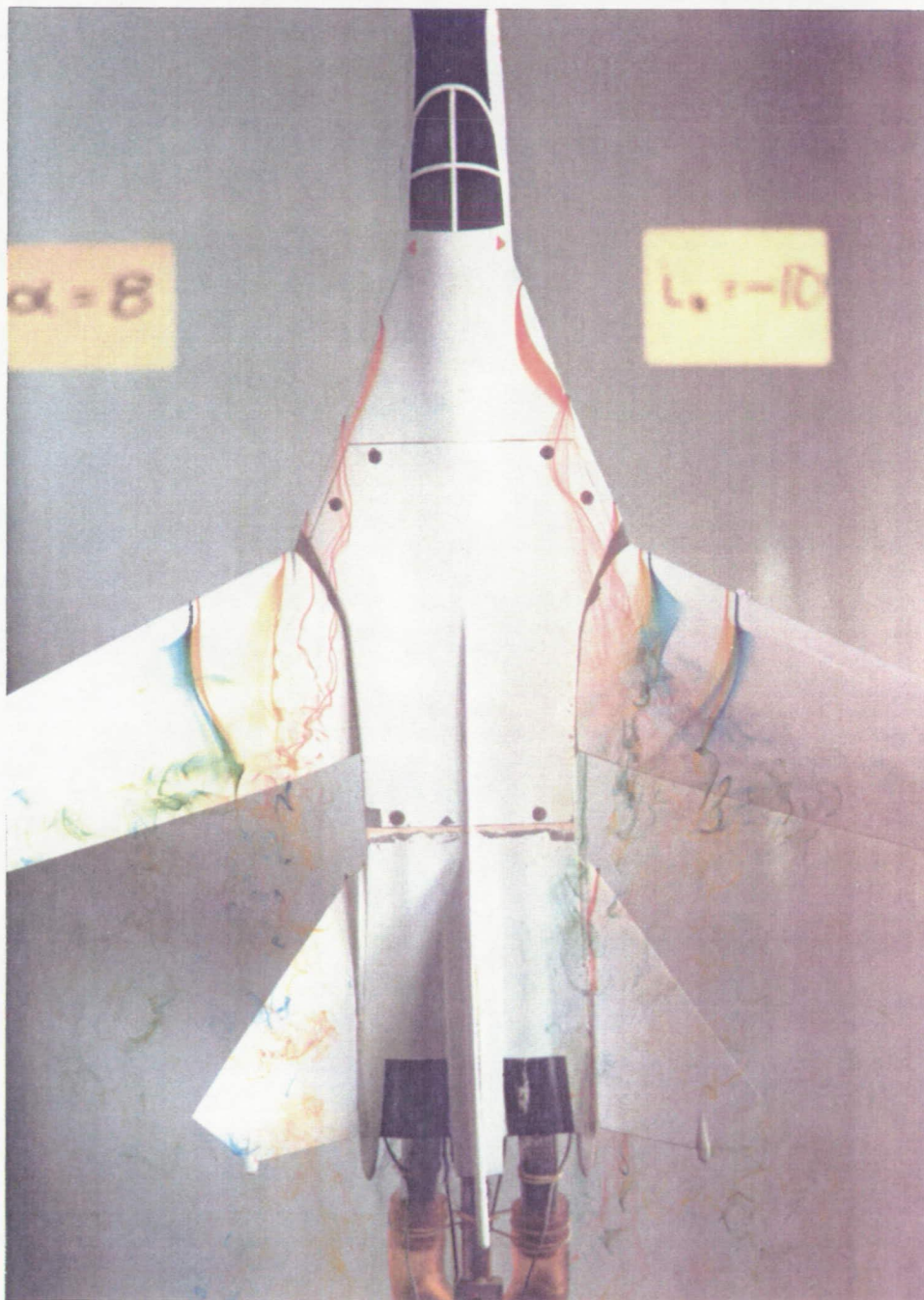
EC90 143-12

(a) Plan view.

Figure 10. Characteristic flow patterns at $\alpha = 8°$, $\delta_{LE/TE} = 10/2$, and $i_h = -10°$.
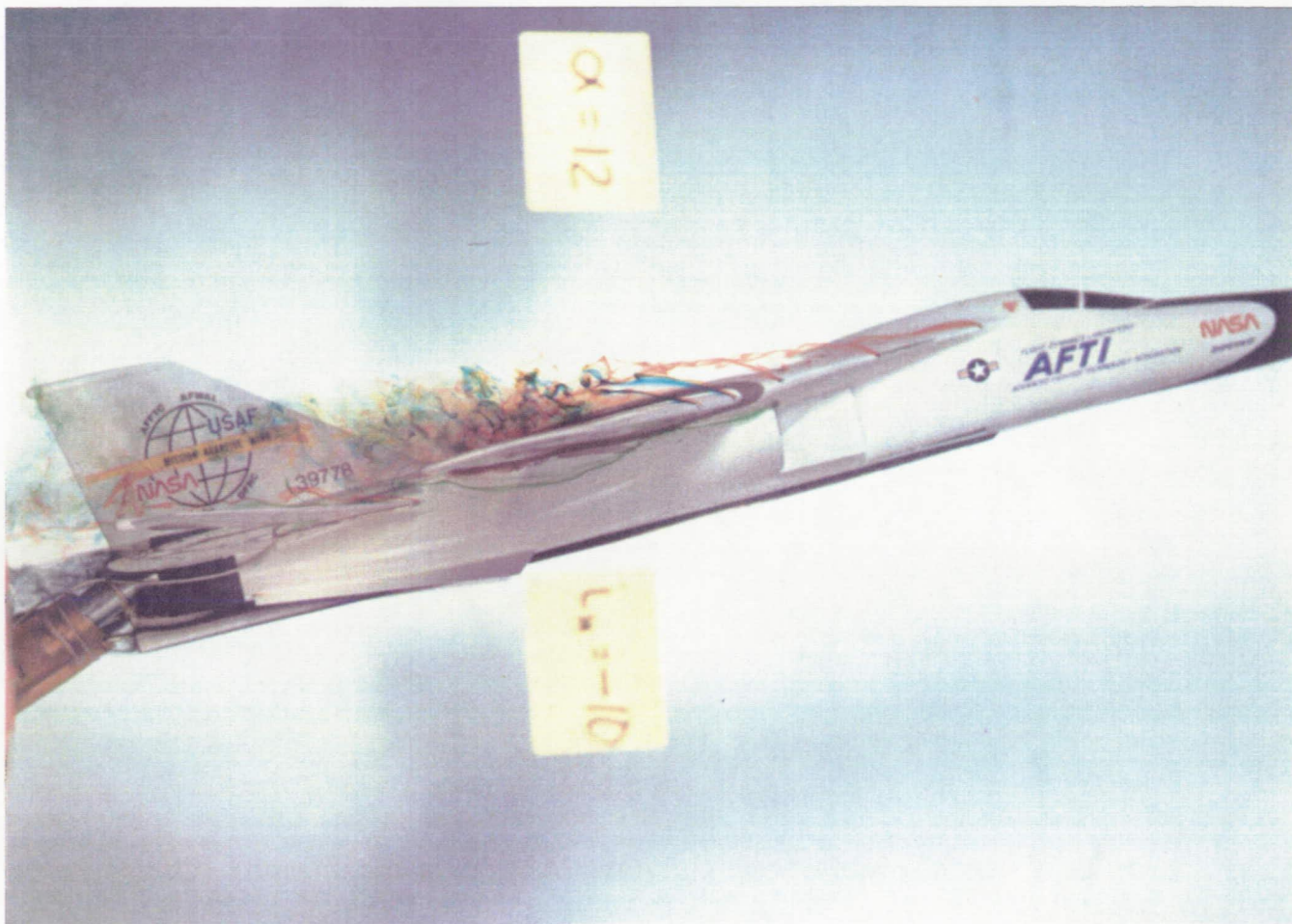
EC90 143-10

(b) Side view.

Figure 10. Concluded.

EC90 143-11

(a) Plan view.

Figure 11. Characteristic flow patterns at $\alpha = 10°$, $\delta_{LE/TE} = 10/2$, and $i_h = -10°$.

EC90 143-14

(b) Side view.

Figure 11. Concluded.

EC90 143-15

(a) Plan view.

Figure 12. Characteristic flow patterns at $\alpha = 12°$, $\delta_{LE/TE} = 10/2$, and $i_h = -10°$.

(b) Side view.

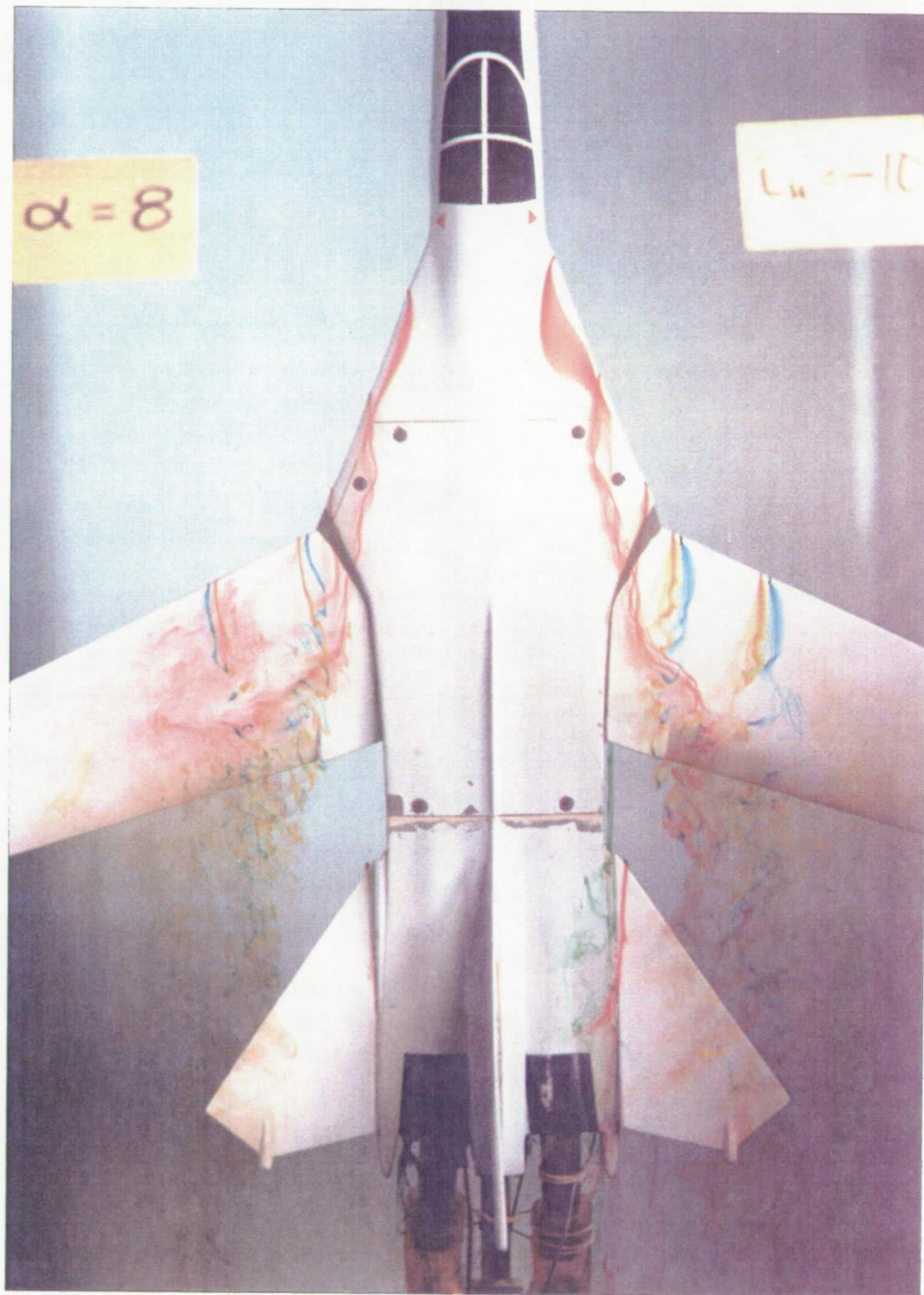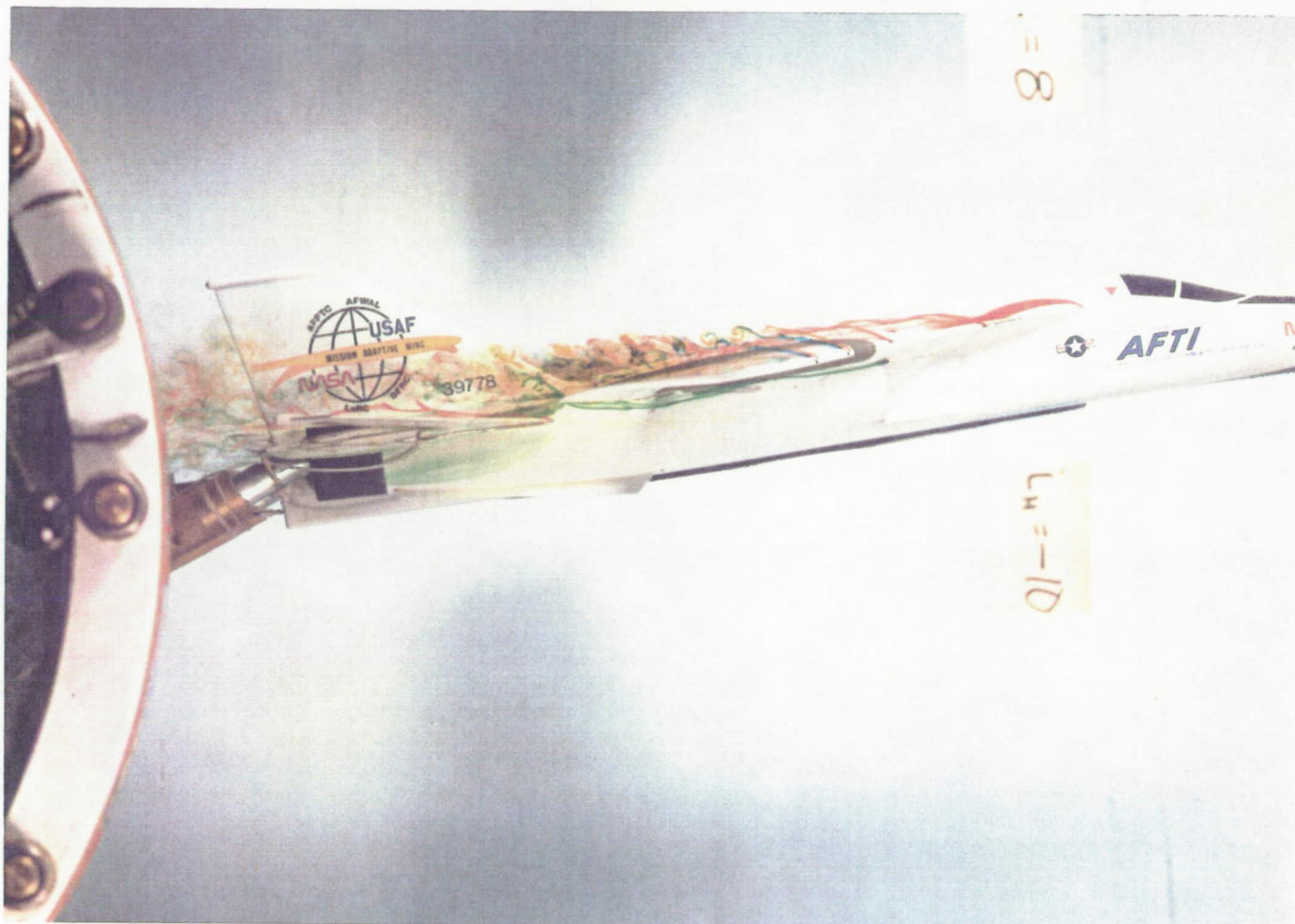Figure 12. Concluded.

EC90 143-13

EC90 143-16

(a) Plan view.

Figure 13. Characteristic flow patterns at $\alpha = 8°$, $\delta_{LE/TE} = 0/10$, and $i_h = -10°$.

EC90 143-17

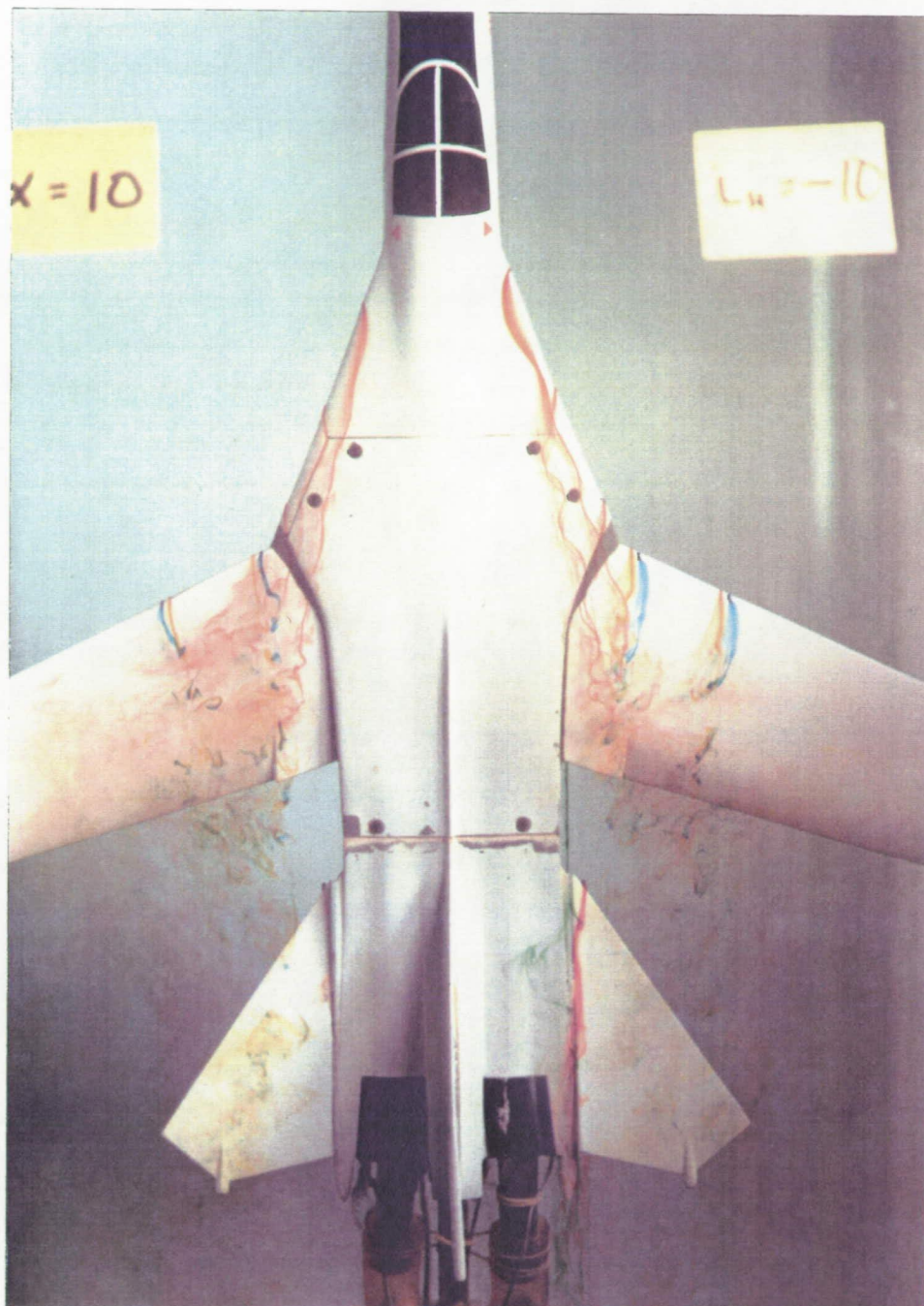(b) Side view.

Figure 13. Concluded.

EC90 143-19

(a) Plan view.

Figure 14. Characteristic flow patterns at $\alpha = 10°$, $\delta_{LE/TE} = 0/10$, and $i_h = -10°$.

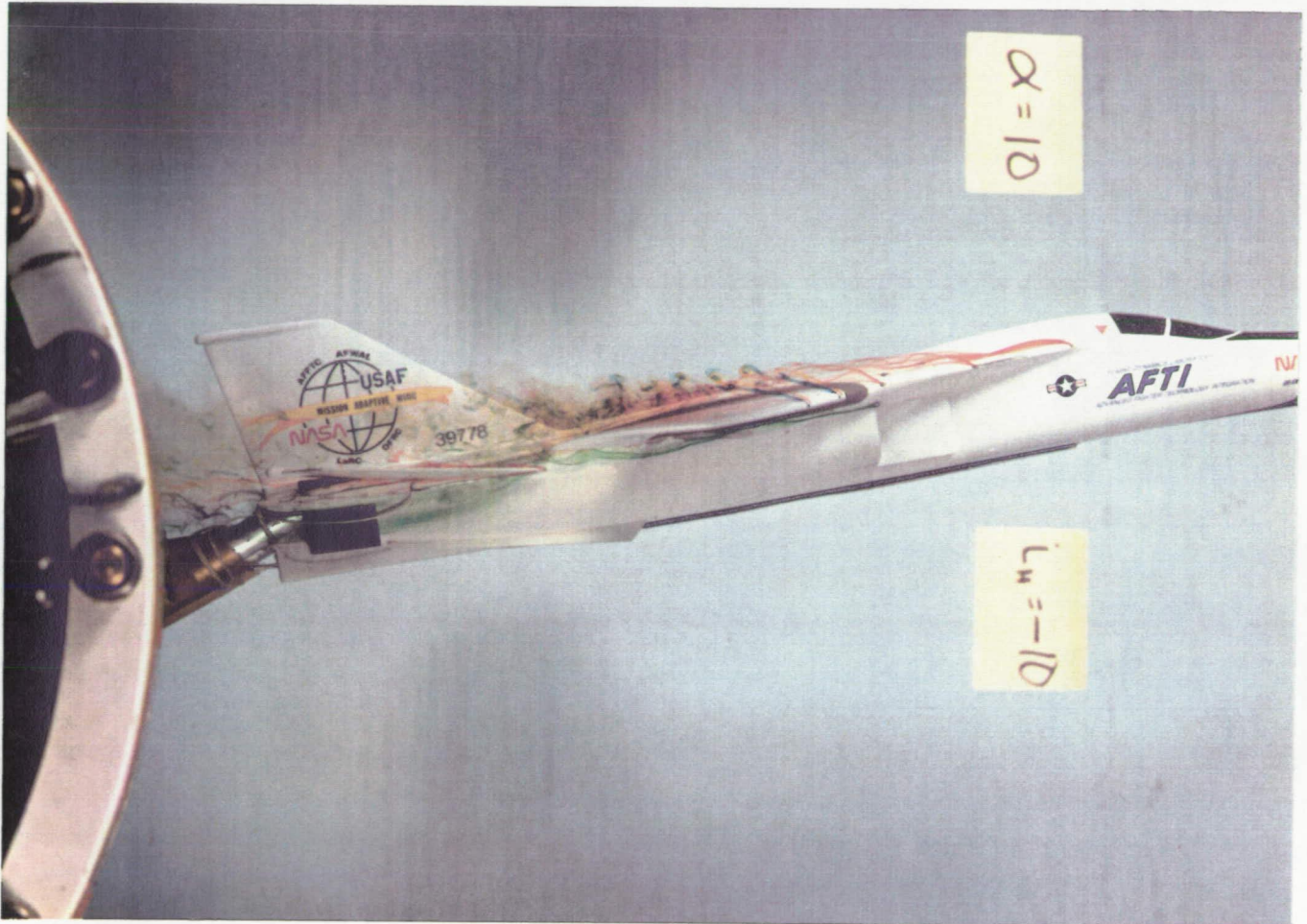α = 10

$i_H = -10$

EC90 143-20

(b) Side view.

Figure 14. Concluded.

31

EC90 143-18

(a) Plan view.

Figure 15. Characteristic flow patterns at $\alpha = 12°$, $\delta_{LE/TE} = 0/10$, and $i_h = -10°$.

EC90 143-21

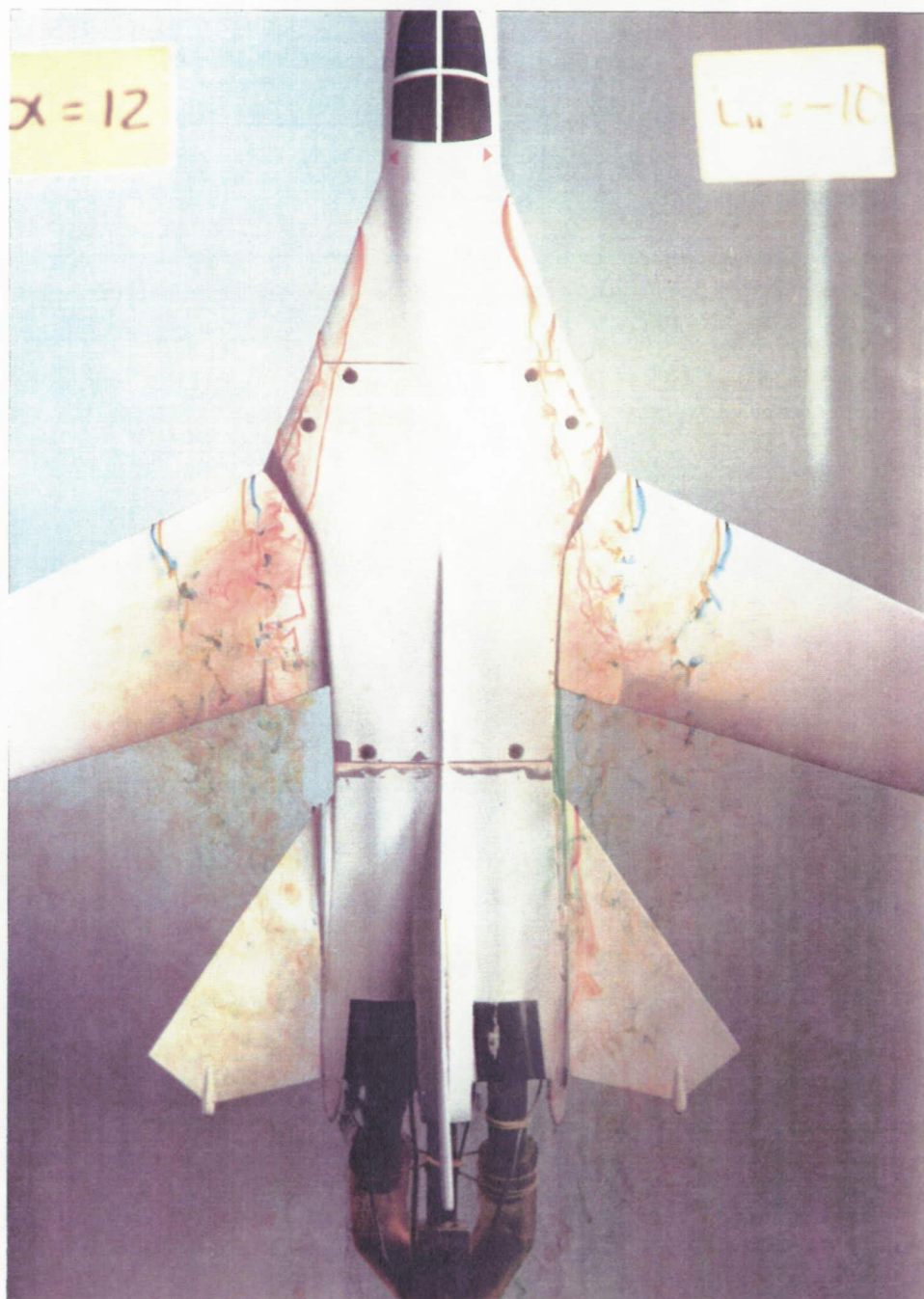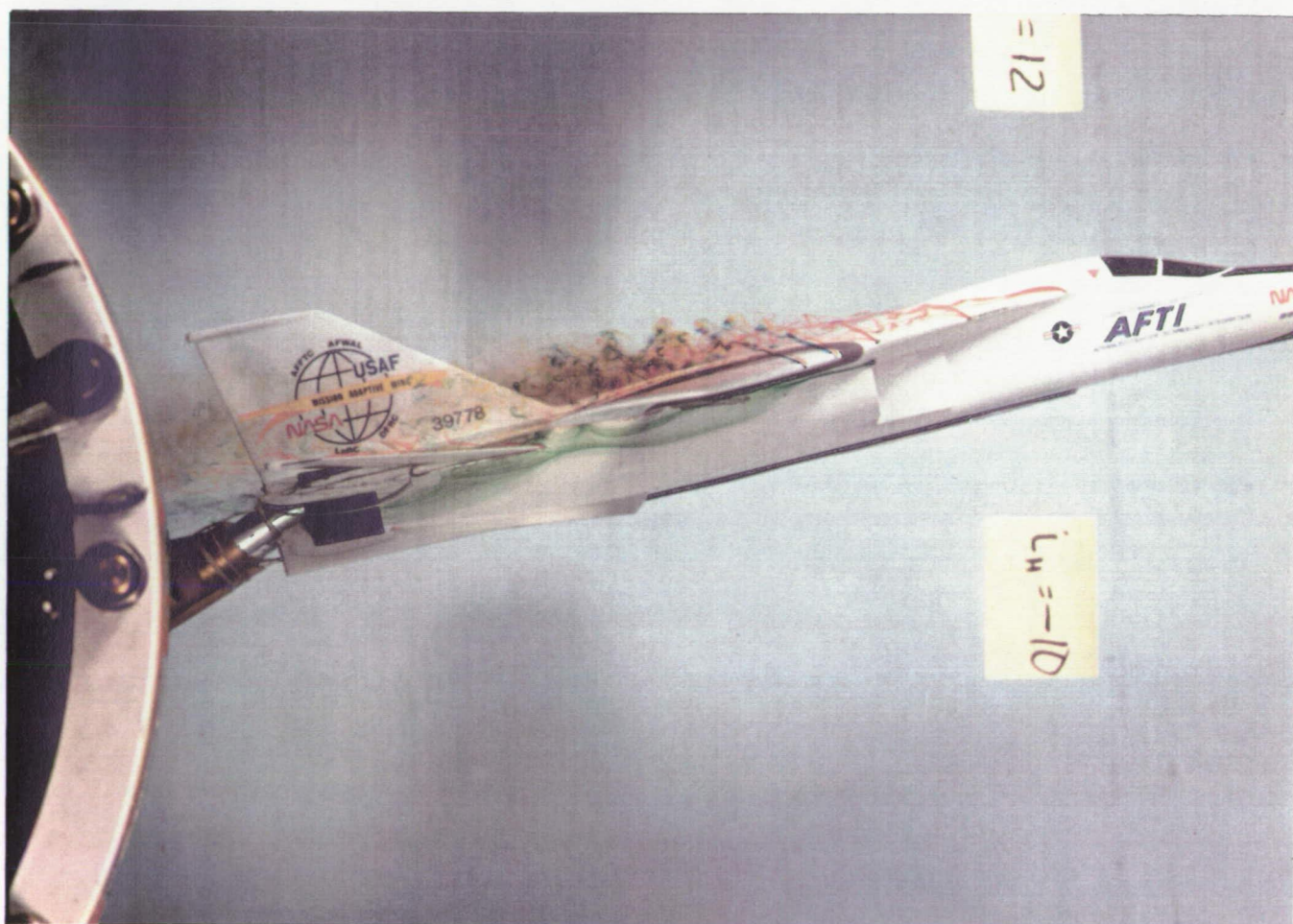(b) Side view.

Figure 15. Concluded.

1. Report No. NASA TM-101698	2. Government Accession No.	3. Recipient's Catalog No.

| 4. Title and Subtitle Flow Visualization Study of a 1/48-Scale AFTI/F111 Model to Investigate Horizontal Tail Flow Disturbances | 5. Report Date June 1991 |
| | 6. Performing Organization Code |

| 7. Author(s) Lisa J. Bjarke | 8. Performing Organization Report No. H-1547 |
| | 10. Work Unit No. RTOP 533-02-11 |

| 9. Performing Organization Name and Address NASA Dryden Flight Research Facility P.O. Box 273 Edwards, California 93523-0273 | 11. Contract or Grant No. |
| | 13. Type of Report and Period Covered Technical Memorandum |

| 12. Sponsoring Agency Name and Address National Aeronautics and Space Administration Washington, DC 20546-3191 | 14. Sponsoring Agency Code |

15. Supplementary Notes

16. Abstract

During flight testing of the AFTI/F111 aircraft, horizontal tail buffet was observed. Flutter analysis ruled out any aeroelastic instability, so a water-tunnel flow visualization study was conducted to investigate possible flow disturbances on the horizontal tail which might cause buffet. For this study, a 1/48-scale model was used. Four different wing cambers and one horizontal tail setting were tested between 0°- and 20°-angle of attack. These wing cambers corresponded to the following leading–trailing-edge deflections: 0/2, 10/10, 10/2, and 0/10. Flow visualization results in the form of still photographs are presented for each of the four wing cambers between 8°- and 12°-angle of attack. In general, the horizontal tail experiences flow disturbances which become more pronounced with angle of attack or wing trailing-edge deflection.

17. Key Words (Suggested by Author(s)) AFTI; Flow visualization; Horizontal tail buffet; Water tunnel	18. Distribution Statement Unclassified — Unlimited Subject category 02

19. Security Classif. (of this report) Unclassified	20. Security Classif. (of this page) Unclassified	21. No. of Pages 37	22. Price A03